OCEANOGRAPHY No. 111, 2011

A regional climate model simulation over the Baltic Sea region for the last Millennium

Semjon Schimanke, Erik Kjellström, Gustav Strandberg, H.E. Markus Meier

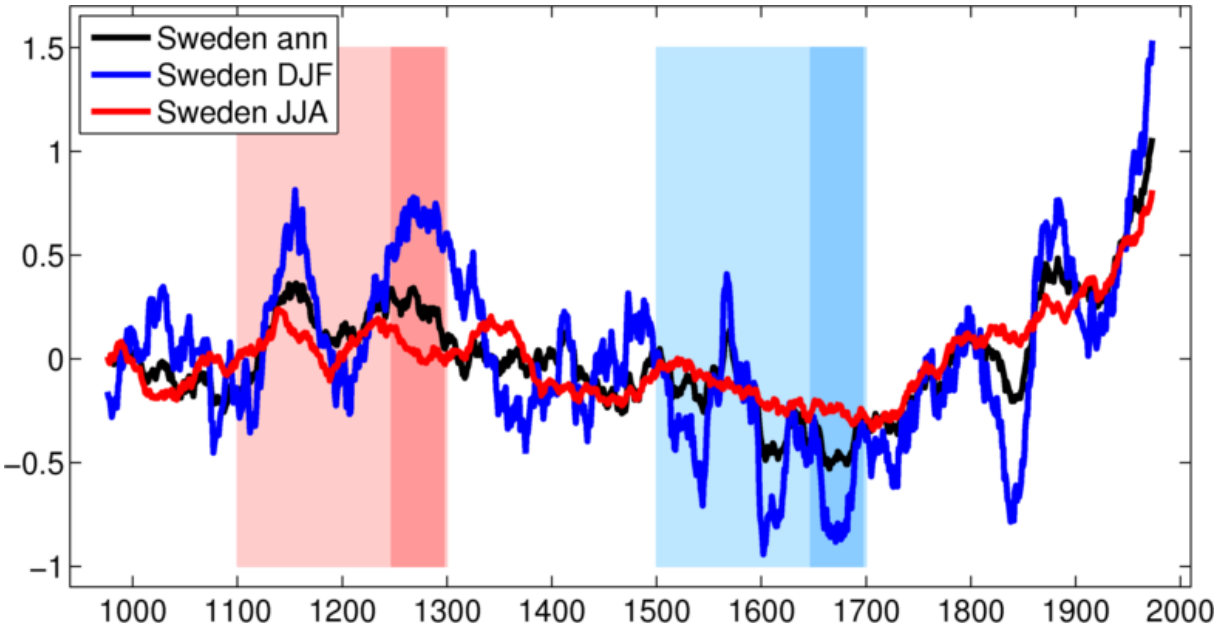

Front:
The temporal evolution of the temperature over Sweden for the complete simulation ranging from 950 A.D. until 1998 A.D. Winter (blue), summer (red) and annual (black) means are illustrated as 50-year running means. The defined periods of the Medieval Climate Anomaly (red) and the Little Ice Age (blue) are highlighted.

ISSN: 0283-7714

OCEANOGRAFI Nr 111, 2011

A regional climate model simulation over the Baltic Sea region for the last Millennium

Semjon Schimanke, Erik Kjellström, Gustav Strandberg, H. E. Markus Meier

Abstract. Variability and long-term climate change in Fennoscandia is investigated in a 1000-year long climate model simulation. We use the Rossby Centre Regional Climate model (RCA3) with boundary conditions from a General Circulation Model (GCM). Solar variability, changes in orbital parameters and changes in greenhouse gases over the last millennium are used to force the climate models. It is shown that RCA3 generates a warm period corresponding to the Medieval Climate Anomaly (MCA) being the warmest period within the millennium apart from the 20th century. Moreover, an analogy for the Little Ice Age (LIA) was shown to be the coldest period. The simulated periods are 1100-1299 A.D. for the MCA and 1600-1799 A.D. for the LIA, respectively. This is in agreement with reconstructions and mostly related to changes in the solar irradiance. We found that multi decadal variability has an important impact on the appearance of the MCA and LIA. Moreover, multi decadal variability may help to explain sometimes contradicting reconstructions if these are representative for relatively short non-overlapping periods. In addition to time series, we investigate spatial patterns of temperature, sea level pressure, precipitation, cloud cover, wind speed and gustiness for annual and seasonal means. Most parameters show the clearest response for the winter season. For instance, winter during the MCA are 1-2.5 K warmer than during the LIA for multi decadal averages.

Sammanfattning. Variabilitet och långsiktig klimatförändring i Fennoskandien undersöks i en 1000 år lång under det senaste milleniet i en 1000 år lång klimatmodellsimulering. Vi använder Rossby Centres regionala klimatmodell (RCA3) med randvärden från en global klimatmodell (GCM). Effekten av variabilitet i solinstrålning, ändrade astronomiska förhållanden och ändringar i växthusgskoncentrationer har använts för att driva modellerna. Resultaten visar att RCA3 genererar en medeltida varm period (MCA) som är den varmaste under hela milleniet undantaget 1900-talet. Dessutom visar resultaten på en kall ”Lilla Istid” (LIA). I simuleringen motsvarar dessa perioder 1100-1299 (MCA) samt 1600-1799 (LIA). Det här överensstämmer med rekonstruktioner och kan till största delen relateras till ändringar i solinstrålning. Vi fann vidare att variabiliteten över flera decennier har en betydande effekt på klimatet under MCA och LIA. Variabiliteten över flera decennier kan ibland också förklara motsägelsefulla rekonstruktioner om dessa är representativa för kortare icke sammanfallande perioder. I tillägg till tidsserier, undersöker vi också rumsliga mönster hos temperatur, lufttryck i havsytans nivå, nederbörd, molntäcke, vindhastighet och byighet för både säsongs- och årsmedelvärden. De flesta parametrarna visar störst skillnad mellan olika perioder för vintersäsongen. Som exempel kan nämnas att vintern under MCA var 1-2.5 K varmare än under LIA sett som medelvärde över flera decennier.

1. Introduction

The climate of the last millennium is characterised by large long term variability. Reconstructions reveal cooler and warmer centuries. Warmer conditions are found at the beginning of the last millennium with cooler conditions thereafter [*Xoplaki et al.*, 2011]. This climate variability is unaffected from any strong man-made climate change which does not start until approximately 1850. Most studies reveal that such long term variability can be triggered from the sun [e.g. *Haigh*, 1996] since the suns irradiation varies over different time scales from days till millennia [*Lean*, 2005]. Beside changes in temperature other parameters were effected as shifts in storm tracks, precipitation and cloudiness [*Xoplaki et al.*, 2011]. Such general statements are mostly valid for the global or hemispheric scale while patterns become patchy and ambiguous when changes on regional scales are investigated.

Starting with the definitions of the warm and cold periods - normally known as the Medieval Climate Anomaly (MCA) and the Little Ice Age (LIA)- is already puzzling. Some definitions used in other studies are summarised in the following list:

- MCA
  - 950-1250 [*Mann et al.*, 2009]
  - 1080-1280 [*Steinhilber and Beer*, 2011]
  - 950-1100 [*Xoplaki et al.*, 2011, page 13]
  - 900-1400 [*Xoplaki et al.*, 2011, page 14]
  - 900-1250 [*Jungclaus et al.*, 2010]
- LIA
  - 1400-1700 [*Mann et al.*, 2009]
  - 1350-1850 [*Steinhilber and Beer*, 2011]
  - 1500-1850 [*Jungclaus et al.*, 2010]

The variety of definitions for the MCA and the LIA gives a first impression that these events are vague. Talking about proxy data the variety is even larger since the signal does not vary only in time but also in space. Here, a short overview on previous results mainly based on tree ring data is given in comparison to model results.

Results from proxy and model studies in a general and global perspective can be summarised as the MCA was warm and the LIA was cool [*Xoplaki et al.*, 2011]. Moreover, there is evidence from different studies that during the MCA a strong La Niña like pattern was prevailing, this influenced the climate in large parts of world by teleconnections [*Mann et al.*, 2009]. Exceptions from the La Niña influence were Europe and perhaps North Africa [*Xoplaki et al.*, 2011]. In these areas, a positive NAO phase appears to have been the dominating factor for climate variations during MCA [*Mann et al.*, 2009; *Xoplaki et al.*, 2011]. With respect to model simulations so far no model is able to reproduce the reconstructed La Niña anomaly [*Mann et al.*, 2009; *Xoplaki et al.*, 2011]. For the European area, only a model with an improved vertical resolution including the stratosphere reflects the reconstructed SLP anomaly pattern [*Mann et al.*, 2009] corresponding to a positive NAO phase. The importance of the stratosphere to capture the European signal during LIA is also highlighted in other model studies [e.g. *Spangehl et al.*, 2010]. However, since most models are not able to reproduce the reconstructed MCA patterns (especially the La Niña like response) several studies suggested that MCA patterns could have been largely influenced by purely internal, natural variability [e.g. *Mann et al.*, 2009; *Jungclaus et al.*, 2010; *Hünicke et al.*, 2010].

Reconstructions based on proxy data reveal a variety for different periods and regions. Note, that listed results refer mainly to tree ring based analyses. These are for temperature as well as precipitation mostly restricted to the summer and/or the early vegetation period [*Xoplaki et al.*, 2011]. Trees are mainly sensitive to the growing season temperature and it is not expected that trees in the region can provide precipitation information with the same accuracy as for the temperature. Regarding precipitation, associations can be found only with spring or early summer [*Linderholm et al.*, 2010]. For summer temperatures correlations higher than 0.85 over Fennoscandia were found while for precipitation data from tree rings the explained variance was only 31% in a Finnish and 25% in a Swedish study [*Linderholm et al.*, 2010]. Regarding the data basis of tree rings it is worth noting, that globally less than 30 tree ring chronologies extend back over the past 1000 years. And three span more than 6000 years [*Linderholm et al.*, 2010]. Although the amount of data is still rather small significant differences between MCA and LIA are included [*Linderholm et al.*, 2010].

In terms of spring/summer precipitation most proxy studies agree that the MCA was generally drier whereas LIA (or overall cold periods) was wetter in north-

ern/central Europe [pages 14-15 *Xoplaki et al.*, 2011]. However, on the multi-decadal time scale a high variability exists as well in general drier or wetter conditions. *Helama and Lindholm* [2003] reported that within the dry MCA the period 1081-1095 was one of the three wettest periods in their 1000 year record.

In summer and winter, both reconstructions and simulations with data assimilation show a clear warm period in Europe between 900 and 1050 AD during the MCA [*Xoplaki et al.*, 2011]. Summer temperatures in Lapland over the last 1250 years underwent the warmest and coolest 250 years periods from AD 931-1180 and AD 1601-1850, respectively [*Helama et al.*, 2009b].

Recent studies reveal also sunshine anomalies from tree ring data. Here, for Northern Scandinavia the coldest century of LIA (April-August) is also the sunniest century (July-August). While during the warmest phase of MCA (950-1100 AD) the summers were unusually cloudy [*Gagen et al.*, 2011]. Similar results were found in simulations with the general circulation model (hereafter GCM) ECHO-G [*Legutke and Voss*, 1999]. Here, low temperatures during the Late Maunder Minimum (1680-1710 AD) coincide with stronger downwelling of solar radiation implying sunnier weather. A possible explanation could be that reduced atmospheric water content lead to a reduction of the greenhouse effect [*Gagen et al.*, 2011].

Another important point for the understanding of changing patterns is the role of the NAO during different seasons. Most studies focus on the NAO during the winter period where the influence is strongest on European climate. Investigating the influence of a summer NAO (SNAO) *Folland et al.* [2009] stated that a positive SNAO is associated with warm and dry conditions over North West Europe and cooler and wetter in southern Europe. They found low SNAO indices from 1650-1750 and around 1800 and strong positive since 1970. Note that their time series does not include the MCA.

Following *Hense and Glowienka-Hense* [2008] the Swedish winter/spring temperature is correlated with the NAO phase. For precipitation, only for the Norwegian mountains and the Mediterranean area a correlation and anti-correlation is found with the NAO index, respectively. But there is no correlation with precipitation over Sweden [*Hense and Glowienka-Hense*, 2008].

In this study we focus on the sensitive Baltic Sea region including most parts of Northern Europe and examine the solar influence and the variability on different time scales onto this region. As introduced, there are some reconstructions available, mainly based on tree rings, which cover the last millennium. However, due to the spatial and temporal sparse density of reconstructions many questions cannot be answered yet. On the other hand, the usage of GCMs cannot reflect local changes. A common technique to achieve information at the local/regional scale is to perform so called dynamically downscaling by using a regional climate model operating at high horizontal resolution [e.g. *Rummukainen*, 2010]. Therefore, we use the regional climate model RCA3 (Rossby Centre Regional Climate model) to downscale the last 1000 years from a simulation of the Holocene with the ECHO-G GCM. Furthermore, we concentrate on atmospheric parameters important for the Baltic Sea as e.g. changes in runoff, wind speed, and gustiness.

In the next section the models, the parameters and methods are briefly introduced. In the third section results of annual and seasonal mean changes of atmospheric key parameters are presented and discussed. Finally, conclusions of the study are highlighted and discussed.

2. Models, data and methods

2.1. Experimental setup

We use a dynamical downscaling approach to highlight signals over northern Europe. The used GCM is ECHO-G whereas the regional climate model is RCA3 (find model descriptions below). The ECHO-G model is forced with variations in orbital parameters, solar irradiance and greenhouse gases between 7000 BP and 1998 AD. However, the focus in this study is on the last millennium. Therefore, we use only boundary conditions from 950 AD until 1998 AD to force RCA3. A more elaborative description of the ECHO-G Holocene simulation can be found in *Hünicke et al.* [2010].

Figure 1 shows the evolution of the CO_2 concentration and the solar insolation as prescribed for ECHO-G and RCA3. The variability of the CO_2 concentration is relatively small in the pre-industrial period. Until 1850 the CO_2 concentration varies between 270 and 290 ppmv. A rapid increase occurs thereafter which is known to be anthropogenic. Towards the end of the simulation the CO_2 concentration reaches values of more than 360 ppmv.

A variation in the solar radiation appears during the whole millennium. The most distinct minima were the Oort (1050), the Spörer (1450), the Maunder (1700), and the Dalton (1800) minimum. The solar variability is scaled to an insolation difference between present day and the Maunder Minimum of 0.3% as estimated by *Lean et al.* [1995].

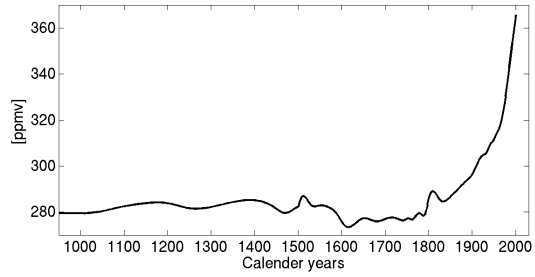

(a) *CO2*

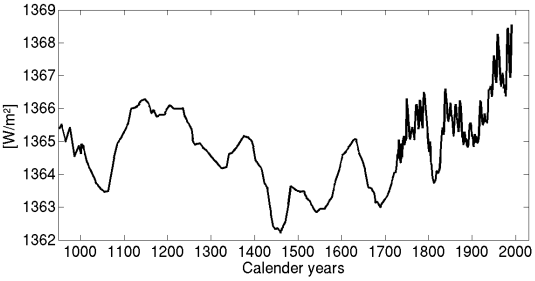

(b) *Solar*

Figure 1. The main forcing parameters of the simulation. (a) Prescribed CO_2 concentrations [ppmv] and (b) solar irradiance [W/m^2].

2.2. Model description

2.2.1. ECHO-G The global climate model ECHO-G [*Legutke and Voss*, 1999] consists of the spectral atmospheric general circulation model (AGCM) ECHAM4 and the coupled ocean-thermodynamic/ dynamic sea ice model HOPE-G. The simulation used to force RCA3 was conducted with a horizontal resolution of T30 (approx. 3.75°x3.75°) and 19 vertical levels. The ocean model HOPE-G has an effective horizontal resolution of approximately 2.8°x2.8° with 20 vertical levels. In the tropical regions a grid refinement is employed with decreasing meridional grid point distance, reaching a value of 0.5° at the equator. The model is flux corrected in order to prevent a climate drift.

2.2.2. RCA3 RCA3 is based on the numerical weather prediction model HIRLAM [*Samuelsson et al.*, 2011]. Whereas lakes are simulated with a lake model the sea surface temperatures (SSTs) are taken from ECHO-G. The model is in good agreement with observations and disagree only slightly if it is forced with ERA40 boundary conditions. The small biases include a too high MSLP in the Mediterranean region, a warm bias in the northeastern part, a cold bias in Southern Europe and North Africa and an underestimation of the diurnal cycle (temperature) [*Samuelsson et al.*, 2011]. Due to the finer resolution the geographical distribution of precipitation is better captured in RCA3 than in the ERA40 reanalysis [*Lind and Kjellström*, 2009; *Samuelsson et al.*, 2011].

In the recent configuration RCA3 has a rotated longitude latitude grid with a resolution of 0.44° (∼50 km) and consists of 102 X 111 grid boxes centred over Europe. Note, that the eight outer limit boxes are used for the relaxation to the boundary conditions supplied by ECHO-G and are therefore not considered in the analysis. In the vertical RCA3 has 24 levels. The time step of the model is 30 min. For a detailed model description we refer to *Samuelsson et al.* [2011].

2.3. Analysed parameters

In this study we focus on annual and seasonal mean changes of some physical parameters necessary to force Baltic Sea models as 2m air temperature, sea level pressure (SLP), precipitation, cloudiness, wind speed, gustiness, maximum wind speed, runoff, and sea surface height (SSH) in the Kattegat.

RCA3 provides two different output parameters for wind extremes: the maximum 10m wind speed and the maximum of estimated gust wind. The maximum 10m wind speed is calculated following the Monin-Obukhov theory and is interpolated from the lowest atmospheric level (90m) down to 10m. The max. estimated gust wind is derived from the turbulent kinetic energy (TKE) equations. Here the gust winds can propagate down to the surface from all boundary layer levels if the mixing is strong enough. For both parameters the absolute maximum over the output interval of 3 hours is stored. In general, the estimated gust wind should be larger than the maximum 10m wind speed.

2.4. Definition of inflows

The literature agrees upon the dependency of salt water inflows on atmospheric conditions over the North Sea [*Matthäus*, 2006, and references therein]. However, inflows are finally defined only by the amount of salty water entering the Baltic Sea [e.g. *Meier and Kauker*, 2003]. The common definition is based on empirical criteria at the Darss Sill. *Franck et al.* [1987] employed the thresholds

$$S_o/S_b \geq 0.8 \text{ and } S_b \geq 17psu$$

to identify the events with the surface salinity S_o and the bottom salinity S_b. Since we are not using an ocean model we cannot use this common definition.

Therefore, we have to fall back on the relationship between SLP gradients and sea surface height to estimate the amount and strength of inflows in our simulations. *Gustafsson and Andersson* [2001] point out that changes in SLP explain more than 70% of the SSH variance in the Kattegat. Therefore, we developed an algorithm based only on SLP gradients to identify inflows.

2.4.1. The inflows of 1993 and 2003 For the design of the algorithm we investigate the development of SLP gradients during two observed major events: The inflow of January 1993 which was according to *Gustafsson and Andersson* [2001] the strongest inflow during the last century and the major event of the winter 2002/2003. In terms of SLP differences between Oksøy (Norway, 58.17°N and 8.00°E) and De Bilt (Netherlands, 52.12°N and 5.18°E) these events are illustrated in Figure 2. Note that these figures as well as the whole development of the algorithm are based on the RCA3 simulation forced with ERA40 boundary conditions to be able to compare the results with observation.

While the mean pressure difference between Oksøy and De Bilt is -2.9 hPa (therefore a westerly wind) inflows depend on fluctuations in this gradient. To get strong inflows first a westward flow is needed to lower the sea level of the Baltic Sea and consequently remove a large quantity of water. This must be followed by strong westerlies which leads to an increase of SSH and a barotropic inflow of salty water from the North Sea. It is known from observations that the easterly and westerly phase lasts approximately 20 days each [*Lass and Matthäus*, 1996].

However, in Figure 2 it becomes obvious that this differs from event to event. One of the strongest inflows of the last century (January 1993, Fig. 2a) is not induced by strong easterlies. The 20 day running mean (red curve) is hardly positive at all. Only a few days at the end of 1992 reveal slightly positive SLP gradients according to easterly winds. On the other hand, the following period with westerlies is characterised by a phase of very strong negative SLP gradients. The 20 day mean minimum is -17 hPa. This is the absolute minimum over the whole considered time period (1961-2009). The daily mean minimum of -27.8 hPa is the second lowest (lowest appeared in February 1962). Therefore, this event is not characterised by a strong outflow phase at the beginning but by very strong westerlies during the inflow phase. Even without a considerable outflow phase this event belongs to one of the seven very strong major inflow since the beginning of observations in 1880 [*Matthäus*, 2006].

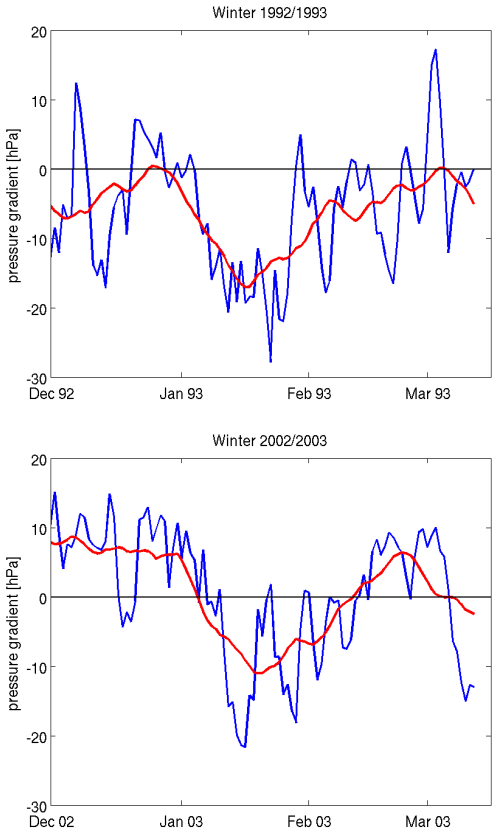

Figure 2. SLP differences [hPa] between Oksøy (Norway) and De Bilt (Netherlands). Blue lines indicate daily values. Red lines show the 20 day running mean. Figures are for the major inflows in January 1993 (top) and January 2003 (bottom).

The event of January 2003 is characterised by a long and persistent outflow phase. The 20 day running mean reaches values close to 10 hPa with single day values around 15 hPa. Accordingly, the Baltic Sea water level was low at the end of this period. The subsequent change to westerlies accrued abruptly and for some days the pressure difference was below -20 hPa. However, the inflow phase was not as persistent as during the event of 1993.

2.4.2. The identification algorithm Events are identified on the basis of daily and 20 day running mean SLP differences (see Fig 2 above). This takes high and low frequency variability into account. Since the event of 1993 does not show a considerable phase of easterly winds on lower frequencies we consider for the outflow phase only daily variability. We define that an inflow can occur if at least at one of the prevailing 20 days the

pressure difference is above +3 hPa. Secondly, the inflow phase seems to be characterised by low frequency variability. We define that a considerable inflow can take place if the mean over 20 days is below -10 hPa. As soon as both assumptions are fulfilled it is considered that an event happened. In general, events can be identified from September until May excluding only the summer.

Finally, the strength of an event is defined. Tests turned out that the high frequency variability is not a good measure for the strength. When the total amount of inflow is calculated in studies with an ocean model the duration of an event is considered. Therefore, we define the strength simply by the difference between the maximum of the running mean up to 20 days in advance of an event and the minimum 20 days thereafter.

2.4.3. Comparison with observed inflows The strength of all identified inflows is illustrated in Figure 3. The exact date (year and month) can be found in Table 1. With the chosen parameters the algorithm identifies 51 events in the period from January 1961 until December 2009. Over the entire period this corresponds to approximately 1 event per winter. This is in agreement with frequencies found in observations [e.g. *Matthäus and Franck*, 1992].

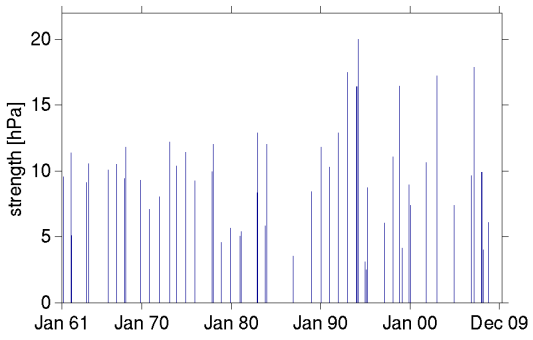

Figure 3. The strength of all identified inflows based on SLP differences between the outflow phase with easterlies and the inflow phase with westerlies. Differences are based on the 20 day running mean. See text for more information.

Moreover, even if the algorithm is allowed to identify inflows between the beginning of September and the end of May it finds them only between October and March. Most events are registered in December followed by January events. This is in line with the findings by *Meier and Kauker* [2002] for observations and modelled inflows. Therefore, the mean statistics are in good agreement with observations.

The comparison of single events reveals mixed results. On one hand, all major events listed by *Gustafsson and Andersson* [2001] are identified with the used algorithm (cf. bolt entries in Table 1). In addition, most of their listed major events are identified with a high amplitude by the algorithm. For example, the inflows in January 1993 and 1994 as well as the inflow in October 1998 has the 2nd to 4th highest amplitudes identified by the algorithm (Fig. 3).

Table 1. 51 major inflow events are identified using SLP gradients over the North Sea. Here, the year and month of the identified events are listed. Bolt dates highlight the eight strongest inflows identified by *Gustafsson and Andersson* [2001] (only until 1998). These were also identified by the algorithm.

1961 1	1970 10	1980 12	**1990 12**	2000 2
1962 1	1971 12	1981 1	1991 12	2001 10
1962 2	1973 1	1982 11	**1993 1**	2003 1
1963 10	**1973 11**	1982 12	**1994 1**	2004 12
1964 1	**1974 12**	1983 10	1994 3	2006 10
1966 3	**1975 12**	1983 12	1994 12	2007 2
1967 3	1977 10	1986 11	1995 2	2008 1
1968 1	1977 12	1988 12	1995 3	2008 2
1968 3	1978 10		**1997 2**	2008 10
1969 10	1979 11		1997 3	
			1998 2	
			1998 10	
			1999 2	
			1999 11	

On the other side, some events are not in good agreement. The strongest inflow according to the atmospheric conditions appeared in March 1994 but no major inflow was registered in the observations. In this case it could be connected to the strong inflow in January which made the conditions unsuitable. Further, a stagnation period without any major inflow was observed between 1983 and 1993 [e.g. *Matthäus*, 2006] but the algorithm identifies five events (December of 1986, 1988, 1990 and 1991 as well as January 1990). However, some of these events have a low amplitude and the gap in 1990s is the largest in the whole time series (Fig. 3).

3. Results

In this section we will briefly describe the climate state of the model for the recent past (December 1969 until November 1998). The comparison with a simulation forced with ERA40 discloses the model biases

corresponding to the ECHO-G boundary conditions. Then, an overview over the modelled millennium is given by showing time series for relevant parameters (section 3.2). This is followed by a comparison with proxies. In section 3.4 we examine the identified periods of the MCA and the LIA in more detail. Finally, the human influence at the end of the last millennium is briefly discussed.

3.1. Simulated climate at the end of the 20^{th} century

In the following, the climate state and biases during the recent period are investigated. Therefore, the simulation forced with ECHO-G is compared with an RCA3 simulation forced with ERA40 boundary conditions. This reanalysis-driven simulation has earlier been shown to be a good representation of the real state of the atmosphere [*Samuelsson et al.*, 2011]. For all seasons and for the annual mean the periods December 1969 until November 1998 are compared (Figures 4 to 10).

To keep errors small a realistic representation of the large scale circulation is necessary. This corresponds to the spatial pattern of SLP (Fig. 4). The annual mean distribution shows the characteristic low pressure around Iceland and high pressure over Spain and the Mediterranean. The north-south pressure gradient reduces towards the east in the model domain. It is present during all seasons whereas it is strongest during winter and weak during summer.

The overall pattern is similar in the simulation forced with ERA40 (Fig. 4 a-e) and ECHO-G (Fig. 4 f-j), respectively. However, there are considerable differences if the patterns are examined more carefully. For all seasons SLP is underestimated in the southern Baltic Sea when compared to the control run (Fig. 4 k-o). Towards the North and South SLP is overestimated. This general behaviour changes only slightly during different periods and therefore reflects the annual mean. The maximum error can be found during winter at the northern boundary of the model area, the northern tip of Fennoscandia. Here, SLP is overestimated by more than 7 hPa. In combination with the underestimation of SLP in southern Sweden and Denmark the pressure gradient is reduced by approximately 10 hPa between northern and southern Scandinavia. The errors in the MSLP pattern implies that the westerlies over Fennoscandia are too weak on average. Correspondingly, the westerlies further south in central/western Europe are too strong.

The simulated temperature patterns show a decrease of temperatures from the South towards the North in all seasons over Europe (Fig. 5 a-j). The amplitude of the seasonal cycle increases with latitude and the reduction of marine influence. Consequently, the smallest amplitude can be found over the Atlantic.

The underestimation of the westerly flow leads to a cold bias at the northern edge of the Baltic Sea during winter by roughly 3K (Fig. 5 k-o). The amplitude increases towards the North and the East with maximum errors greater than 7K. On the other hand, the stronger zonal flow increases winter temperatures over central Europe (+1.5K). During the other seasons the biases are smaller since the Atlantic influence of the temperature is reduced. The main feature is a slight cold bias in most of the model domain in the order of 1-2K. In the annual mean, different biases cancel each other. In central Europe the annual mean bias is only between 0 to 1K whereas in northern Fennoscandia it is close to 2K.

A special behaviour can be seen over the Baltic Sea as well as parts of the Mediterranean Sea. This behaviour is connected to the prescribted SSTs interpolated from ECHO-G. During winter the temperature over the Bothnian Bay is higher even if all surrounding land surfaces are cooler. The maximum deviation to the control simulation accounts to more than 4K (Fig. 5 k). A somewhat weaker but also positive anomaly can be found from the Kattegat to the Arkoner Sea and over the White Sea. The surface temperatures of the big lakes included in the model domain (e.g. Vänern, Ladoga and Onega) are modelled with a lake model. The winter temperatures over lakes generally differ more (e.g. 5 K Ladoga and Onega Sea) than the corresponding temperatures over land surfaces compared to the control simulation. For the summer season the differences between the two runs over water surfaces are opposite to the winter situation, e.g. colder (more than 5 K) over the Baltic Sea and warmer over the lakes. Only for the White Sea again a positive bias is found. In summary, the seasonal temperature cycle over the Baltic Sea is underestimated with too warm winters and too cold summers.

Regions with climatological high precipitation rates (large scale plus convective precipitation) are generally over the Atlantic and the British Isles. But the highest amount of precipitation can be found in elevated regions as the Alps and the Norwegian mountains (Fig. 6 a-j). A clear seasonal cycle can be found in the West with more precipitation over the Atlantic in fall and winter. Towards the East and the North the opposite is true, with more precipitation during summer. That is due to

convective precipitation during summer which is mainly absent in winter. It is also worth to note that there is a clear land sea contrast in the Baltic Sea region. Especially in spring and summer the heat capacity of the Baltic Sea dampens the temperature cycle (both on seasonal and daily time scales) and therefore leads to more stable conditions over the sea with reduced precipitation as a consequence.

Biases in total precipitation can also be related to SLP biases. Especially in the area of negative SLP anomalies the precipitation is enhanced (Fig. 6). The main areas with more precipitation than in the ERA40 driven run are central Europe, southern Scandinavia and the southern part of eastern Europe. The percental differences are large and span over all seasons. A surplus of more than 20% is found for large areas in the annual mean. During winter and autumn the differences is partly exceeding 50%. On the other hand, precipitation is lower in the Mediterranean area and the Norwegian mountains.

Focusing on the catchment area of the Baltic Sea a general overestimation of precipitation is simulated. The signal decreases towards northeast ranging between +25 and +5% (Fig. 6 o). Especially during winter the difference seems to be enhanced over the Baltic Sea. It is likely that this is connected to warmer SST which leads to more precipitation.

The percentage of total cloud cover increases in general from the South towards the North (Fig. 7 a-j). The climatological cloud cover ranges from partly less than 30% in the southern part of the domain to more than 80% over the Atlantic and Finland/northern Russia depending on the season. To some extent differences between the Baltic Sea and the surrounding land are visible with a tendency of fewer clouds over the sea. It should be noted that the cloud cover at the boundary of the model domain is not realistic and is connected with the model setup. The cloud fraction is set to zero at the outer point of the RCA [*Samuelsson et al.*, 2011]. Even omitting the eigth point relaxation zone (as is done in all figures) a steep gradient is visible along most of the model boundary. This feature is partly represented in the climatological precipitation as well. Therefore, signals at the margin should be considered only carefully.

Cloud cover differences between the two runs are in line with those in precipitation and large scale circulation patterns (Fig. 7 k-o). One exception is the larger fraction of total clouds in the Mediterranean during summer while precipitation is lower. Nevertheless, the larger cloud cover corresponds to the lower temperatures. This is remarkable since the SLP anomaly reflects an increased advection from the Southwest which should bring warmer and more humid air masses. Therefore, the reduction of insolation outweighs the circulation anomaly leading to the decrease of temperatures. As a consequence of lower temperatures precipitation is reduced since convective precipitation dominates in this area.

Highest wind speeds can be found in regions with strong pressure gradients in combination with low surface friction (as over the ocean) (Fig. 8 a-j). Therefore, the maximum mean 10m wind speed is located over the Atlantic west of the British isles. In relation with the seasonal cycle of SLP patterns the wind is strongest in winter over most of the model domain. Most parts of Scandinavia (except Norway) are characterised by low wind speeds during all seasons only partly exceeding 3 m/s.

Biases in the 10m wind speed are unequal in space. An overestimation in wind speed can be found in the southern Baltic area whereas wind speed is underestimated in the northern part (Fig. 8 k-o). This, once more, reflects SLP biases. Biases range between +0.5 and -0.5 m/s with greatest anomalies during winter. Stronger biases are present over sea surface areas with high temperature biases, e.g. over the Bothnian Bay during winter.

The general pattern of gustiness (as well as maximum 10m wind speed which will not be discussed separately) mirrors the mean 10m wind fields. Therefore, the bias patterns for gustiness (Fig. 9) and maximum 10m wind speed (Fig. 10) look quite similar to the biases of the mean 10m wind speed. More pronounced gustiness is found over most parts of the southern Baltic area in winter and spring compared to that in the ERA40 driven simulation. During summer and autumn, the area with underestimated gustiness is more extended. Stronger differences over the Baltic Sea area can be explained by lower stability connected to the higher 2m air temperature. This enhances vertical mixing and therefore the gustiness.

3.2. Time series

3.2.1. Temperature evolution during the last millennium Figure 11a+b) illustrates the temporal evolution of the Swedish mean temperature during the whole simulation as 50 year running means. Beside the annual mean we show the evolution for all seasons. Apart from the anthropogenic signal at the end of the simulation the smoothed annual mean differs never more than 0.5 K from the long-term mean. Fluctuations of summer values are smaller while winter varia-

tions are larger. During the transition seasons the variability is somewhat higher than in the annual mean at the beginning of the simulation. In the second half of the simulation the temporal evolution is astonishingly close to the annual mean. In general, anomalies in the annual mean is mainly driven by changes in winter temperatures since these have the largest amplitude. For example, the cold peaks in the 16th century are connected to the winter anomalies only while there is no clear signal in any other season (Fig. 11a+b).

The warmest period in the pre-industrial area is found in the 12th and 13th centuries. The coldest period is simulated in the 17th and 18th centuries. These periods are defined as MCA and LIA in this study. This is in agreement with definitions of other studies (see introduction). The anomalies are forced mainly by solar variability but strongly interfere with internal multidecadal variability since the fluctuations are higher than suspected by natural forcing alone. Beside the annual mean this prevails for all seasons but with different amplitudes. The main signal is attributed to the winter while considerable smaller amplitudes are found especially in summer and spring.

Comparing maxima and minima of the 50 year running mean in the pre-industrial period (until 1800 AD) we find greatest differences between 1.75 K and 0.58 K for winter and summer, respectively. The maximum annual mean signal is 0.89 K. All maxima and minima in all seasons fall within the defined MCA (1100-1299) and LIA (1600-1799) periods. The only exception is the spring minimum which occurs already before the defined MCA. But note, that the spring anomaly during LIA is clearly negative as well. Furthermore, MCA and LIA consist not of a single peak but have multiple peaks due to the internal long term variability (Fig. 11a+b).

An additional minimum is found in the 19th century. Here, once more the strongest signal can be found especially for the running winter mean and partly for spring temperatures. This minimum coincides approximately with the solar Dalton minimum (Fig. 1 b). However, the minimum is astonishing low and very sharp. Most climate models simulate only a clear Dalton minimum if volcano eruptions are considered [*Wagner and Zorita*, 2005]. That is not the case in the ECHO-G simulation. Therefore, it cannot be excluded that the signal is to a great extent connected to internal variability. On the other hand, it is also possible that small forcings amplify through positive internal feedbacks (e.g. ice albedo feedback) on the regional scale (personal communication Sebastian Wagner).

Figure 11c) illustrates the temporal evolution of the temperature for a grid point close to Stockholm (located at 59.22N and 18.33E) and over the Baltic Sea (in the Baltic proper east of Gotland, 57.01N and 19.52E). Both anomalies vary quite close to each other for annual as well as winter means. Only, the response over the sea is mostly damped. There are only few exceptions. The second temperature minimum during LIA is deeper for Stockholm than for the Baltic Sea. This is true also for the minimum during the Dalton minimum.

3.2.2. SLP gradients, inflow events, runoff and SSH The SLP gradient over the North Sea is a key parameter for the SSH in the Kattegat which steers the inflow of saline water from the North Sea into the Baltic Sea [*Meier and Kauker*, 2003]. Furthermore, the transport of maritime air masses from the North Atlantic towards Scandinavia is related to the SLP gradient partly controlling temperature anomalies. Figure 12a) shows the 50 year running mean SLP differences between De Bilt and Oksøy for annual, winter, and summer means. The mean SLP gradient is close to 3 hPa in the annual mean and generally stronger in winter (3.5 hPa) than in summer (2.2 hPa). However, there is considerable amount of variability during the millennium.

Wintertime SLP gradients are generally stronger during MCA compared to LIA. Therefore, the link between SLP gradients and the temperature response seems to exist also in this simulation. The high temperatures close to 1300 AD correspond to the strongest peak in SLP gradient while weak pressure gradients around 1600 are connected with low temperatures. But, there is no overall correlation of SLP gradients and temperature. Both the second temperature minimum during LIA (around 1670 AD) as well as the Dalton minimum (around 1850) appears more or less independent from emphasised SLP gradients. During the Dalton minimum the SLP gradient is on a level comparable to the peak value of MCA whereas the Swedish mean temperature is close to the absolute minimum. Apparently, the SLP gradient over the North Sea cannot explain all variations and other mechanisms must be involved. We have to keep in mind that we do not compare to the NAO index which would probably encounter for more of the variability. Moreover, according to *Kauker and Meier* [2003] other patterns than the NAO are important as well.

Figure 12 b) illustrates the strength of inflows summarised over 20 year periods. The strength is based on the pressure gradient over the North Sea (chapter 2.4.2). There is a general correlation between the strength of inflows and the SLP gradient during winter. Higher

pressure gradients at the beginning of the last millennium are correlated with stronger inflows while a reduced SLP gradient during LIA produces weaker inflows. Especially, the decrease of the SLP gradient and the strength of inflows starting around 1300 and lasting until 1700 is in very good agreement. In general, the algorithm based on SLP gradients indicates that the mean strength of inflows was higher during MCA than LIA.

The sea surface height in the Kattegat can be estimated by SLP gradients over the North Sea [*Gustafsson and Andersson*, 2001]. This has been done following the definition by *Meier et al.* [2011]. Therefore, SLP gradients and SSH are highly correlated as expected (Fig.12 c).

The runoff is estimated from the net water budget (precipitation minus evaporation) over the Baltic drainage area using a statistical model (see *Meier et al.* [2011] for more information). It is illustrated in Fig. 12 d) in combination with precipitation only. Runoff and precipitation are considerable higher during the MCA than in the LIA. The peak runoff during the MCA is approximately 800 m^3/s (+6%) higher than in the LIA. The development is in agreement with changes in SLP gradients.

Table 2. Linear correlation coefficients for yearly means (top) and winter (DJF, bottom) means. The computation of correlation is restricted to the pre-industrial area (950-1799) to avoid correlations on the basis of trends in the last 200 years. Correlations are computed for the time series of SLP gradients, precipitation, Scandinavian mean temperature, runoff in the Baltic Sea catchment area and SSH in Kattegat.

	Prec	Temp	Runoff	SSH
SLP	0.482	0.506	0.422	0.994
Prec	-	0.317	0.663	0.479
Temp	-	-	0.281	0.509
Runoff	-	-	-	0.412
SLP	0.526	0.654	-	0.994
Prec	-	0.454	-	-

Linear correlation coefficients between SLP gradients, precipitation, Scandinavian mean temperature, runoff and SSH in the Kattegat are summarised in Table 2. Since the SSH is estimated with SLP gradients a correlation coefficient close to 1 is achieved for annual and winter means. The yearly runoff is strongest correlated to precipitation in the catchment area (correlation is 0.66) whereas the relation to temperature is weaker (correlation is 0.28). Moreover, the strength of the oceanic influence based on SLP gradients has an impact on the mean runoff. Here, the correlation coefficient has a value of 0.42. It is only a little bit higher if precipitation is considered directly (0.48). However, as stated in the introduction the impact of SLP gradients over the Atlantic is more relevant for the Scandinavian temperature than for the precipitation. In terms of linear correlation coefficients we find a correlation of 0.53 for precipitation and 0.65 for temperature during winter (DJF).

3.3. Comparison with proxies and observations

A rigorous comparison with proxy data is difficult to accomplish due to the paucity of high-quality data covering the European continent. Observational data, historical evidence and proxy-based data do exist and in some cases the records encompass the entire millennium. Most proxy data relates to the temperature climate during summer. Proxies representative of winter conditions are fewer and do not date that far back in time. Other complications with comparison to proxy- and or observational data are that the current model simulation lacks the impact from changes in both volcanic forcing and tropospheric aerosols. The former is important as strong volcanic eruptions can have a strong impact on the temperature climate [e.g. *Guiot et al.*, 2010]. Examples from the historic time include the eruptions of Tambora in 1815, Krakatoa in 1883 and Pinatubo in 1991. This effect is mostly on a relatively short time scale of up to a few years and on decadal to multi-decadal time scales other forcing factors, like changes in the solar forcing, becomes more important [e.g. *Shindell et al.*, 2003]. Tropospheric aerosols tend to dampen the strong 20th century warming due to increasing greenhouse gases in the atmosphere both by directly scattering incoming solar radiation back to space, but also by modifying cloud properties. As the aerosol effect is neglected in the ECHO-G simulation there is a very strong increase in global mean temperature in the 20th century. Keeping the above mentioned problems with model-proxy comparisons in mind, we give two examples of such comparisons in the following; one for summertime temperatures and one for the relation between large-scale atmospheric circulation and wintertime temperatures.

First we note that the Europe-wide summer temperature climate shows a large degree of both inter-annual and decadal variability in the proxy-based record from *Guiot et al.* [2010], see Figure 13. Starting out from warm conditions, a long cooling follows until c. 1600 only interrupted by a warm anomaly in the mid 16th

century. After a strong warming in the 17th century the long-term temperature is relatively constant with exception to cold events in the late 17th century and the end of the 19th century. The latter is followed by a warming in the first half of the 20th century and then there is a strong warming also in the most recent decades. The inter-annual and decadal variability are of similar size in the proxy-based reconstruction as in the model simulation in the pre-industrial period (i.e. prior to c. 1850). In the latter part of the record, however, the model simulates a strong positive trend not reflected in the proxy-based data. As mentioned above, part of this strong trend is likely due to the lack of changing tropospheric aerosol forcing with time. In the model, many years in the last 50 years of the simulations are warmer than any years in previous periods of the entire millennium. Also in the proxy-based data the last decades are warm but there are also years equally warm, or even warmer, in earlier parts of the Millennium.

Large-scale circulation and temperature climate As discussed above, the atmospheric large-scale circulation determines to a large degree the climate in the northern European region. Here we compare the large-scale atmospheric circulation, as described by the NAO index, with data on 2m-temperature. The comparisons are done both for the model simulation and for proxy-based data. The proxy-data on the NAO index is taken from the reconstruction of *Luterbacher et al.* [2002] dating back to 1500. These data represents seasonal mean conditions and we focus first on winter (December, January and February). Here, we compare it to the model NAO index based on model simulated mean sea level pressure (MSLP) taken from the grid-boxes closest to Lisbon and Reykjavik. To derive the index based on model data we first normalise the year-to-year anomalies w.r.t to the long-term average with the long-term inter-annual standard deviation. This is done for both grid boxes based on the full time series. For the winter climate we compare the December-February NAO index to temperatures from Stockholm representing average January-April conditions. The proxy data series is based on ice break-up data from Stockholm harbour *Leijonhufvud et al.* [2009]. It starts in 1502 and continues until 2008 with only 13 years of lacking data, all during the first 50 years. In the following NAO-temperature comparisons we restrict the analysis in all four data sets to the time period 1502-1998.

The north-south pressure gradient as given by the NAO index shows a large degree of inter-annual variability in the proxy-based data for winter (Fig. 13). There is also long-term variability on decadal to multi-decadal time scales, e.g. a high-index period in the 18th century. The model shows slightly larger inter-annual variability (standard deviation of the full time series is 1.81 vs 1.63 for the proxy-based data) and somewhat weaker multi-decadal variability (standard deviations of 30-year running averages is 0.29 vs 0.35), Fig. 14b). More extreme situations, i.e. winters with NAO on average exceeds plus/minus 2, are slightly more frequent in the model (71 vs 57 for negative anomalies, and 58 vs 53 for positive).

Figures 14 a) and b) also show temperature data for Stockholm and it is clearly seen that there is a correlation between a high NAO index and high winter/spring temperatures in both model and proxies. The correlation coefficients are 0.53 and 0.49 for RCA3 and the proxy data respectively in terms of inter-annual variability. For multi-decadal time scales the correlation is 0.79 for the proxy data while only 0.49 for the model. This relatively low correlation in the model is due to the strong temperature trend in the 20th century that is not directly related to changes in the atmospheric circulation. The degree of correlation increases to 0.76 if we constrain the analysis to the time period prior to 1900 in the model data.

3.4. MCA and LIA pattern

In the following we analyse the regional patterns in northern Europe corresponding to the Swedish temperature anomalies during MCA and LIA. Therefore, we examine differences between MCA and LIA each a 200 year long period. Additionally, we investigate 50 year extreme periods. Here, we take 1246-1295 and 1647-1696 as maximum and minimum within MCA and LIA, respectively (see Fig. 11. In addition to the differences the mean over the pre-industrial period (950-1800 AD) is shown.

3.4.1. Differences between the full MCA and LIA periods As we defined our MCA and LIA periods by warm and cold phases found in the running mean (Fig. 11) we see a clear signal in the spatial pattern of the temperature differences. In correspondence to stronger winter amplitudes in the running mean we find the greatest differences in the spatial pattern during winter (Fig. 15 f-j). The temperature difference increases from zero at the southern tip of the Baltic Sea to 1 K in northern Fennoscandia. Over the Baltic Sea the mean winter signal has the order of 0.4 K. During spring and autumn the general pattern is similar with the exception that the amplitude is approximately only half of it. The signal is almost non existing for the summer season.

Most proxy and model studies (see introduction) suggest that warm and cold anomalies are connected with changes in the NAO index - at least during winter. This is also indicated by the interannual and multi decadal variability discussed for Stockholm above (section 3.3). However, concerning the full 200-year periods we cannot see a clear SLP signal in our simulation (Fig. 16 f-j). During winter when the relationship is supposed to be strongest we find only a small reduction of 0.5 hPa over Iceland but no increase towards the south. Therefore, there is no NAO signal which can explain the temperature signal during MCA in comparison to the LIA. There is only a small signal during spring (MAM, Fig. 16 g). SLP anomalies resemble a slightly negative NAO pattern. The pressure gradient is reduced in the order of 1 hPa. In northern Scandinavia this is connected to a slight warming since the prevailing continental influence during spring with cold air is reduced (Fig. 15 g). There is only very little SLP response during summer and autumn.

Differences in precipitation are in general only of minor size between the 200 years periods (Fig. 17 f-j). Most of Fennoscandia is slightly wetter during MCA but the relative change in the annual mean never exceeds 4%. A large part can be traced back to changes in autumn and winter whereas the spring was drier in MCA than during LIA. This is the case especially in southern Scandinavia with a maximum reduction of up to 8% (Fig. 17 g). That is a consequence of the reduced maritime influence in line with the negative NAO phase during spring.

Since the differences in the SLP patterns are only minor, large signals for the 10m wind speed cannot be expected. A slight increase is found for the MCA with local maxima of 0.2 m/s over the Baltic Sea (Fig. 18 f-j). That is only of minor size compared to the mean wind speed of 5-7 m/s.

The amplitudes of differences in the gustiness are somewhat higher and have a similar pattern than wind speed anomalies (Fig. 19 f-j). However, the differences are small and not pronounced. The difference in the maximum 10m wind speed is even less in the comparison between both 200 years periods (Fig. 20 f-j).

A reliable difference in total cloud cover cannot be identified in any season or the annual mean (Fig. 21).

3.4.2. Differences between the 50 extreme years within MCA and LIA There exist a quite high variability within the full 200 years periods of the MCA and LIA on different time scales (Fig. 11 and 12). Therefore, we select special periods to estimate the full range of variability between the MCA and LIA. We choose the warmest 50 years period from MCA (1246-1295) and compare it with the coldest 50 years period of LIA (1647-1696, see Fig. 11). This implies that the signal is larger than for the comparison of the full MCA and LIA periods. Note that the signal of these 50 year periods is also part of the full periods.

The winter mean temperatures over Scandinavia differ regionally between 1 and 2.5 K over Fennoscandia when both extreme periods are compared (Fig. 15 k-o). The amplitude increases once more from the Southwest towards the Northeast. In spring and autumn the pattern remains similar only with reduced amplitude. Also in summer an overall warming can be seen but of small amplitude (0.3 K over land and 0.5 K over the Baltic Sea). This was not the case for the full periods. Moreover, the maximum warming appears to be shifted towards central Europe in summer.

The SLP anomalies between the extreme periods are quite different when compared to the full periods (Fig. 16). In winter, a clear positive NAO anomaly is simulated for MCA even if the pressure reduction is shifted towards northern Scandinavia. That is one reason for increased winter temperatures as well as enhanced winter precipitation over large areas. The documented NAO negative phase during spring is different in shape for the 50 year periods and more restricted to the Atlantic Ocean. During summer SLP changes are only minor before during autumn the positive NAO phase develops. The annual mean resembles a positive NAO phase.

As stated for the full periods the precipitation is higher during the MCA than in the LIA in winter. For the 50-year periods this holds true for spring and autumn as well. In large areas the increase amounts to more than 10%. The signal is less clear during summer where regions with a reduction of precipitation can be found as well - especially over the Baltic Sea (Fig. 17). Nevertheless, the annual mean shows that the warmest 50 years during MCA are connected with more precipitation as indicated already in the 50-year running mean (Fig. 12).

A clear signal can be seen in mean wind speed (Fig. 18), gustiness (Fig. 19), and the maximum 10m wind speed (Fig. 20) over the southern Baltic Sea in winter and spring. The mean wind speed is enhanced by more than 0.2 m/s in large areas whereas local responses are up to 0.4 m/s. The pattern of the gustiness is similar but with a higher amplitude (more than 0.5 m/s). In summer and autumn a clear response is missing for mean wind speed whereas gustiness is still slightly stronger during the MCA. The annual mean re-

flects an increase in wind speed and gustiness and is in agreement with changes in SLP patterns. From changes in the SLP field it can be deduced that it is mainly the westerly component which is stronger during the MCA.

There is no remarkable signal in the total cloud cover. Even the increase in precipitation is not reflected in terms of cloud cover. Changes in cloud cover never exceed a difference of 4% (Fig. 21 k-o).

3.5. Climate change in the 20th century

Observations indicate a clear rise of the global mean temperature throughout the last century [*IPCC*, 2007]. It is demonstrated that this warming is most likely triggered by the anthropogenic increase of greenhouse gas concentrations [*IPCC*, 2007]. The increase of GHG concentrations is one of the main forcings in the used GCM simulation (see Fig. 1). Therefore, an increase of the temperature is simulated in the model. Nevertheless, the raise of 1 K until 1998 in the 50 year running mean (Fig. 11 a+b) is too strong when compared to measurements and other simulations. This is likely due to the omission of increasing aerosol concentrations which have a cooling effect and partly counteract the global warming [*IPCC*, 2007].

There are also rather strong changes in the other parameters beside the temperature (Fig. 12). These include increasing SLP gradients over the North Sea and an extraordinary increase of precipitation and runoff. In how far such changes are realistic is not further examined.

Finally, the experimental setup was not supposed to demonstrate the human made climate change in the 20th century. Hence, this time period is not analysed in detail.

4. Discussion

4.1. Temperature

The temporal evolution of the temperature over northern Europe is in general in good agreement with observations and reconstructions during the pre-industrial period of the last millennium. The strongest simulated warming can be found between 1100 and 1300 AD. This corresponds to the results gathered from proxy data [e.g. *Xoplaki et al.*, 2011] or model studies [*Mann et al.*, 2009]. However, some of the MCA studies include a wider range of years back to 900 AD. *Helama et al.* [2009b] show that the summer temperatures in Lapland over the last 1250 years underwent the warmest 250 years periods from AD 931-1180. Note that the simulation does not reach that far back in time to consider the early stage of the MCA.

The LIA is as well captured in the simulation and is in agreement with other studies in terms of the temperature response. One of the coldest multi-decadal periods was experienced at the end of the 17th century consistent with *Luterbacher et al.* [2004]. Moreover, the temperature signal is greater during winter than during summer. When the full periods for MCA and LIA are considered there is hardly any signal in summer temperatures whereas the winter were colder by 0.4 K during the LIA. *Luterbacher et al.* [2004] show that the European winter temperatures were reduced by 0.5 K from 1500-1900 compared to the 20th century whereas no signal was found for summer temperatures.

A stronger contrast between the MCA and LIA can be found when 50-year extreme periods are considered. This highlights that the natural internal multi-decadal variability played an important role for the characteristics of these periods as stated by *Mann et al.* [2009].

Besides the MCA and LIA signals the temperature decrease at the beginning of the 19th century is remarkable. The running mean winter temperature is close to the minima of the LIA (Fig. 11). It is connected to the reduction of solar activity during the Dalton minimum [*Steinhilber and Beer*, 2011]. However, the temperature decrease is very high compared to other studies [e.g. *Wagner and Zorita*, 2005; *Spangehl et al.*, 2010]. The reason is not fully understood but could be related to internal regional feedbacks.

4.2. SLP

Considering the full MCA and LIA periods we cannot see a clear signal for SLP. However, a negative NAO phase is identified for the LIA compared to the MCA during the 50 year extreme periods. This SLP pattern is in agreement with other model studies [*Spangehl et al.*, 2010] and reconstructions [*Luterbacher et al.*, 2002] in shape and amplitude. This change in the large scale distribution of SLP is the main source for the temperature signal as well as for other parameters.

4.3. Precipitation

The atmospheric circulation connected with a negative (positive) winter NAO displays weaker (stronger) westerly winds. Depending on the strength of the westerlies the amount of warm and humid air coming from the Atlantic to northern Europe varies [*Xoplaki et al.*, 2011]. Accordingly we find a wetter MCA and a drier LIA in terms of total precipitation. Once again, the

Table 3. Reconstruction of precipitation in different studies. Blue colours indicate wet periods whereas red colours highlight dry periods. All studies report changes in Fennoscandia with the exception of *Xoplaki et al.* [2011] reporting general anomalies in the European region (including e.g. Mediterranean, the Alps and Fennoscandia. Furthermore, all studies present anomalies for the early growing season (mostly May-July) whereas *Linderholm and Chen* [2005] reports winter anomalies.

	900-1099	1100-1299	1300-1499	1500-1699	1700-1899
Helama and Lindholm [2003]	1081-1095	1173-1191	1388-1402 1433-1447	1664-1680	1752-1765
Linderholm and Chen [2005]				1565-1620, 1690- 1520-1560	-1730, 1890-1950 1730-1850
Helama et al. [2009a]	950-	-1220 1220-	1300-1499	1500-1650	
Jönsson and Nilsson [2009]				1560-1590 1657-1675	1694-1751 1753-1832
Xoplaki et al. [2011], pages 14-15	1000-	-1200 1200-	-1400		

signal is much clearer for the 50-year periods with an increase of total precipitation of roughly 6% in the annual mean (compared 1% for the full periods, Fig. 17). However, the signal becomes significantly weaker during summer with even negative anomalies over the Baltic Sea and southern Finland. Therefore, a comparison with reconstructed precipitation anomalies becomes challenging especially since reconstructions itself have a wide range. An short summary of reconstructed precipitation anomalies can be found in Table 3.

Xoplaki et al. [2011] (page 15) state for Europe that the early MCA (they refer to 1000-1200) was drier, followed by a wet period (13th and 14th century). This is partly confirmed by a study focusing on precipitation anomalies in Finland indicating droughts between 1173-1191, 1388-1402, and 1664-1680 [*Helama and Lindholm*, 2003]. Further investigations lead to the conclusion of a mega-drought from the early 11th to the 12th centuries [*Helama et al.*, 2009a]. On the other hand, it was wetter during the periods 1081-1095, 1433-1447, and 1752-1765 [*Helama and Lindholm*, 2003] or more general from 1220-1650 [*Helama et al.*, 2009a]. Especially for Sweden, *Jönsson and Nilsson* [2009] find low precipitation from 1560 to 1590 and during the late Maunder Minimum (1694-1751). Therefore, beside some agreements there are discrepancies. For instance, *Helama et al.* [2009a] document a wet period from 1220-1650 while *Jönsson and Nilsson* [2009] report reduced precipitation from 1560 to 1590. These discussed results refer to the early growing season (mostly May-July).

Results for winter precipitation since 1500 in western central Scandinavia indicate wet conditions during 1520-1560, 1730-1850, and since 1950 [*Linderholm and Chen*, 2005]. Furthermore, *Linderholm and Chen* [2005] supposed that it was drier in the periods 1565-1620, 1690-1730, and 1890-1950.

Therefore, there are both studies supporting and disagreeing with our simulated findings. A further look on the precipitation running mean helps to judge the distinctions (Fig. 12). Some periods are relatively dry within the wetter MCA whereas there is a clear maximum (end of 16th century) in precipitation during the LIA. As a consequence we find only a clear signal for the 50-year periods. This is strongly depending on multi-decadal variability. Perhaps, results from proxy data are affected by high variability as well leading to the disagreement between the studies.

4.4. Inflows

The aim of our research is to find an explanation for the increase in hypoxia during the MCA as reconstructed from sediment cores [e.g. *Zillén and Conley*, 2010]. Since inflows from the North Sea are crucial for the bottom oxygen concentrations a method was defined to identify major inflows based on SLP gradients

between De Bilt and Oksøy. There is evidence that the summed strength of inflows was higher during the MCA than in the LIA. In combination with increased surface temperatures and a reduction of salinity due to higher runoff the increased inflow of salty water could have strengthen the vertical stratification. As a consequence the vertical mixing could have been reduced leading to a reduction of oxygen concentrations and the expansion of hypoxia. However, so far this is only a hypothesis which needs further testing and especially simulations with an ocean model. Moreover, *Zillén and Conley* [2010] argue that human perturbation has been an important factor for hypoxia even during the MCA. Therefore, these open questions should be addressed in the future.

5. Summary

The main conclusions are:

1. The experimental setup is able to reproduce much of the climate variability over the last millennium as documented in observations and reconstructions from proxy data. Only the trend in the 20th century is unrealistic and is therefore not discussed in detail. Moreover, model biases are large at the end of the last century. This is to a large degree related to the boundary conditions from ECHO-G.

2. The temperatures are extraordinary during the MCA and the LIA if the whole pre-industrial period is considered. This highlights the impact of solar variability on the regional scale. Based on the temperature we define the full MCA and LIA periods as 1100-1299 AD and 1600-1799 AD, respectively. This is in the range of specifications based on reconstructions.

3. Internal natural multi-decadal variability plays an important role for the characteristic of the MCA and LIA. In addition to the full periods we investigate extreme periods within the MCA and the LIA. These periods are 1246-1295 AD and 1647-1696 AD, respectively. All parameters show a much clearer signal for the chosen 50 years extreme periods than for the full 200 years time slices. Some parameters do not reveal any difference between the MCA and the LIA if the full periods are considered only.

4. The temperature differences between the MCA and the LIA over Scandinavia during winter range between 0-1 K and 1-2.5 K when full and extreme periods are considered, respectively. These signals are reasonable and have the right order but appear small if compared to the model bias which exceeds locally 4 K in the area of the Baltic Sea. In northern Scandinavia biases are even larger. Note that biases over the Baltic Sea are strongly related to the interpolation of SSTs from ECHO-G.

5. Differences in precipitation are small (+4% in the annual mean) when the full 200 year periods are considered and during spring even opposite to what is found for the extreme periods. During the extreme periods increase of approximately 10% is seen over the whole year with the exception of summer. Model biases range from +5 to +35% over the Baltic Sea catchment area.

6. The probably most decisive model bias was identified for SLP. Especially during winter the north-south pressure gradient in northern Europe is underestimated by 10 hPa with corresponding biases for temperature, precipitation etc. as described above. The SLP signal of 2 hPa between the extreme periods therefore appear to be relatively small. Nevertheless, the identified positive NAO phase during the MCA is in good agreement with other model studies and proxy data.

7. The wind speed does not differ considerably between full MCA and LIA periods. For the 50 year periods an increase of wind speed and gustiness can be found mostly for winter and spring. The differences are concentrated in the southern part of the Baltic Sea. The changes are about the same size as model biases.

8. Considerable differences could not be identified for cloud cover between the MCA and the LIA.

9. The runoff is larger during the MCA compared to the LIA by 6% as a consequence of increased precipitation.

10. We defined an algorithm based on SLP gradients over the North Sea to identify major inflows into the Baltic Sea. Based on that method we find evidence that the summed strength was higher during the MCA than in the LIA.

In summary, clear differences exist only for the 50-year extreme periods whereas the state over the 200-year full periods differ only slightly. Even if most differences are similar in size as the model bias they appear

reasonable since the differences are in agreement with reconstructions and observations.

6. Outlook

It is planned and already partly conducted to force the ocean model RCO3 with the boundary conditions taken from the millennium atmospheric run. First, a delta change approach will be used to avoid biases originating from the global model. Secondly, the atmospheric forcing will be applied after a more sophisticated bias correction. Both setups will be used to investigate the causes of hypoxia during the MCA and herewith test the hypothesis drawn in the discussion.

Acknowledgments.

The work presented in this study was jointly funded by the Swedish Environmental Protection Agency (SEPA, ref. no. 08/381), by the Swedish Research Council for Environment, Agricultural Sciences and Spatial Planning (Formas, ref. no. 2008-1885), and the European Community's Seventh Framework Programme (FP/2007-2013) under grant agreement no. 217246 made with the joint Baltic Sea research and development programme BONUS (http://www.bonusportal.org) within the ECOSUPPORT (Advanced modelling tool for scenarios of the Baltic Sea ECOsystem to SUPPORT decision making, http://www.baltex-research.eu/ecosupport) and the INFLOW (Holocene saline water inflow changes into the Baltic Sea, ecosystem responses and future scenarios, http://projects.gtk.fi/inflow/index.html) project. The RCO model simulations were partly performed on the climate computing resources 'Ekman' and 'Vagn' jointly operated by the Centre for High Performance Computing (PDC) at the Royal Institute of Technology (KTH) in Stockholm and the National Supercomputer Centre (NSC) at Linköping University. 'Ekman' and 'Vagn' are funded by a grant from the Knut and Alice Wallenberg foundation.

References

Folland, C. K., J. Knight, H. W. Linderholm, D. Fereday, S. Ineson, and J. W. Hurrell, The Summer North Atlantic Oscillation: Past, Present, and Future, *Journal of Climate*, *22*, 1082–1103, 2009.

Franck, H., W. Matthäus, and R. Sammler, Major inflows of saline water into the Baltic Sea during the present century, *Gerlands Beitr. Geophys.*, *96*, 517–531, 1987.

Gagen, M., E. Zorita, D. McCarroll, G. H. F. Young, H. Grudd, R. Jalkanen, N. J. Loader, I. Robertson, and A. Kirchhefer, Cloud response to summer temperatures in Fennoscandia over the last thousand years, *GRL*, *38*, L05,701, 2011.

Guiot, J., C. Corona, and E. members, Growing season temperatures in europe and climate forcings over the past 1400 years, *PLoS ONE*, *5*, e9972, 2010.

Gustafsson, B. G., and H. C. Andersson, Modelling the exchange of the Baltic Sea from the meridional atmospheric pressure difference across the North Sea, *JGR*, *106*, 19,731–19,744, 2001.

Haigh, J., The Impact of Solar Variability on Climate, *Science*, *272*, 981–984, 1996.

Helama, S., and M. Lindholm, Droughts and rainfall in south-eastern Finland since AD874, inferred from Scots pine ring-widths, *Boreal Environment Research*, *8*, 171–183, 2003.

Helama, S., J. Merilinen, and H. Tuomenvirta, Multicentinnial megadrought in northern Europe coincided with a global El Niño-Southern Oscillation drought pattern during the Medieval Climate Anomaly, *Geology*, *37*, 175–178, 2009a.

Helama, S., M. Timonen, J. Holopainen, M. G. Ogurtsov, K. Mielikinen, M. Eronen, M. Lindholm, and J. Merilinen, Summer temperature variations in Lapland during the Medieval Warm Period and the Little Ice Age relative to natural instability of thermohaline circulation on multi-decadal and multi-centennial scales, *Journal of Quaternary Science*, *24*, 450–456, 2009b.

Hense, A., and R. Glowienka-Hense, Auswirkungen der Nordatlantischen Oszillation, *PROMET*, *34*, 89–94, 2008.

Hünicke, B., E. Zorita, and S. Haeseler, Baltic Holocene climate and regional sea-level change: A statistical analysis of observations, reconstructions and simulations within present and past analogues for future changes, *Final report of the DFG research unit SINCOS-2*, GKSS, Geesthacht, Germany, 2010.

IPCC, *Climate Change, The Physical Science Basis, Contribution of Working Group I to the Fourth Assessment Report of the Intergovernmental Panel on Climate Change*, Solomon, S., D. Qin, M. Manning, Z. Chen, M. Marquis, K. B. Averyt, M. Tignor, H. L. Miller (Eds.), 2007.

Jönsson, K., and C. Nilsson, Scots Pine (pinus sylvestris L.) on Shingle Fields: A Dendrochronologic Reconstruction of Early Summer Precipitation in Mideast Sweden, *Journal of Climate*, *22*, 4710–4722, 2009.

Jungclaus, J., et al., Climate and carbon-cycle variability over the last millenium, *Clim. Past.*, *6*, 723–737, 2010.

Kauker, F., and H. E. M. Meier, Modeling decadal variablility of the Baltic Sea: 1. Reconstructing atmospheric surface data for the period 1902-1998, *JGR*, *108*, 3267, 2003.

Lass, H. U., and W. Matthäus, On temporal wind variations forcing salt water inflows into the Baltic Sea, *Tellus A*, *48*, 663–671, 1996.

Lean, J., Living with a Variable Sun, *Physics Today*, *58*, 32–38, 2005.

Lean, J., J. Beer, and R. Bradley, Reconstruction of solar irridiance since 1610: Implications for climate change, *Geophysical Research Letters*, *22*, 3195–3198, 1995.

Legutke, S., and R. Voss, The Hamburg Atmosphere-Ocean Coupled Circulation Model ECHO-G, *DKRZ-Report*, 1999.

Leijonhufvud, L., R. Wilson, A. Moberg, J. Sderberg, D. Rets, and U. Sderlind, Five centuries of Stockholm winter/spring temperatures reconstructed from documentary evidence and instrumental observations, *Climate Change*, *101*, 109–141, 2009.

Lind, P., and E. Kjellström, Water budget in the Baltic Sea drainage basin: Evaluation of simulated fluxes in a regional climate model, *Boreal Environment Research*, *14*, 56–67, 2009.

Linderholm, H. W., and D. Chen, Central Scandinavian winter precipitation variability during the past five centuries reconstructed from Pinus sylvestris tree rings, *Boreas*, *34*, 43–52, 2005.

Linderholm, H. W., J. A. Bjrklund, K. Seftigen, B. E. Gunnarson, H. Grudd, J.-H. Jeong, I. Drobyshev, and Y. Liu, Dendroclimatology in fennoscandia from past accomplishments to future potential, *Climate of the Past*, *6*, 93–114, 2010.

Luterbacher, J., E. Xoplaki, D. Dietrich, R. Rickli, J. Jacobeit, C. Beck, D. Gyalistras, C. Schmutz, and H. Wanner, Reconstruction of sea level pressure fields over the Eastern North Atlantic and Europe back to 1500, *Climate Dynamics*, *18*, 545–561, 2002, 10.1007/s00382-001-0196-6.

Luterbacher, J., D. Dietrich, E. Xoplaki, M. Grosjean, and H. Wanner, European Seasonale and Annual Temperature Variability, Trends, and Extremes Since 1500, *Science*, *303*, 1499–1503, 2004.

Mann, M. E., Z. Zhang, S. Rutherford, R. S. Bradley, M. K. Hughes, D. Shindell, C. Ammann, G. Faluvegi, and F. Ni, Global Signatures and Dynamical Origins of the Little Ice Age and Medieval Climate Anomaly, *Science*, *326*, 1256–1260, 2009.

Matthäus, W., *The history of investigations of salt water inflows into the Baltic Sea - from the early beginning to recent results*, Baltic Sea Research Institut (IOW), 65 ed., 2006.

Matthäus, W., and H. Franck, Characteristics of major Baltic inflows - a statistical analysis, *Continental Shelf Research*, *12*, 1375 – 1400, 1992.

Meier, H. E. M., and F. Kauker, Modeling decadal variability of the Baltic Sea: 2. Role of freshwater inflow and large-scale atmospheric circulation for salinity, *Journal of Geophysical Research*, *108*, 3368, 2003.

Meier, H. E. M., H. Andersson, C. Dietrich, K. Eilola, B. Gustafsson, A. Hglund, R. Hordoir, and S. Schimanke, Transient scenario simulations for the Baltic Sea Region during the 21st century, *Tech. rep.*, SMHI, 2011.

Meier, H. M., and F. Kauker, Simulating Baltic Sea climate for the period 1902-1998 with the Rossby Centre coupled ice-ocean model, *Reports Oceanography 30*, SMHI, 2002.

Rummukainen, M., State-of-the-art with regional climate models, *WIRE (Wiley Interdisciplinary Reviews: Climate Change) Advanced Reviews*, *1*, 82–96, 2010.

Samuelsson, P., et al., The Rossby Centre Regional Climate model RCA3: model description and performance, *Tellus*, *63A*, 4–23, 2011.

Shindell, D. T., G. A. Schmidt, R. L. .Miller, and M. E. Mann, Volcanic and Solar Forcing of Climate Change during the Preindustrial Era, *Journal of Climate*, *16*, 4094–4107, 2003.

Spangehl, T., U. Cubasch, C. C. Raible, S. Schimanke, J. Körper, and D. Hofer, Transient climate simulations from the Maunder Minimum to present day: Role of the stratosphere, *JGR*, *115*, 1:18, 2010.

Steinhilber, F., and J. Beer, Solar activity - the past 1200 years, in *Medieval Climate Anomaly*, edited by E. Xoplaki, D. Fleitmann, H. Diaz, L. von Gunten, and T. Kiefer, vol. 19, pp. 5–6, PAGES News, 2011.

Wagner, S., and E. Zorita, The influence of vulcanic, solar and CO2 forcing on the temperatures in the Dalton Minimum (1790-1830): a model study, *Climate Dynamics*, *25*, 205–218, 2005.

Xoplaki, E., D. Fleitmann, H. Diaz, L. von Gunten, and T. Kiefer (Eds.), *Medieval Climate Anomaly*, vol. 19, PAGES News, 2011.

Zillén, L., and D. J. Conley, Hypoxia and cyanobacteria blooms - are they really natural features of the late Holocene history of the Baltic Sea?, *Biogeosciences*, *7*, 2567–2580, 2010.

This preprint was prepared with AGU's LaTeX macros v5.01, with the extension package 'AGU++' by P. W. Daly, version 1.6b from 1999/08/19.

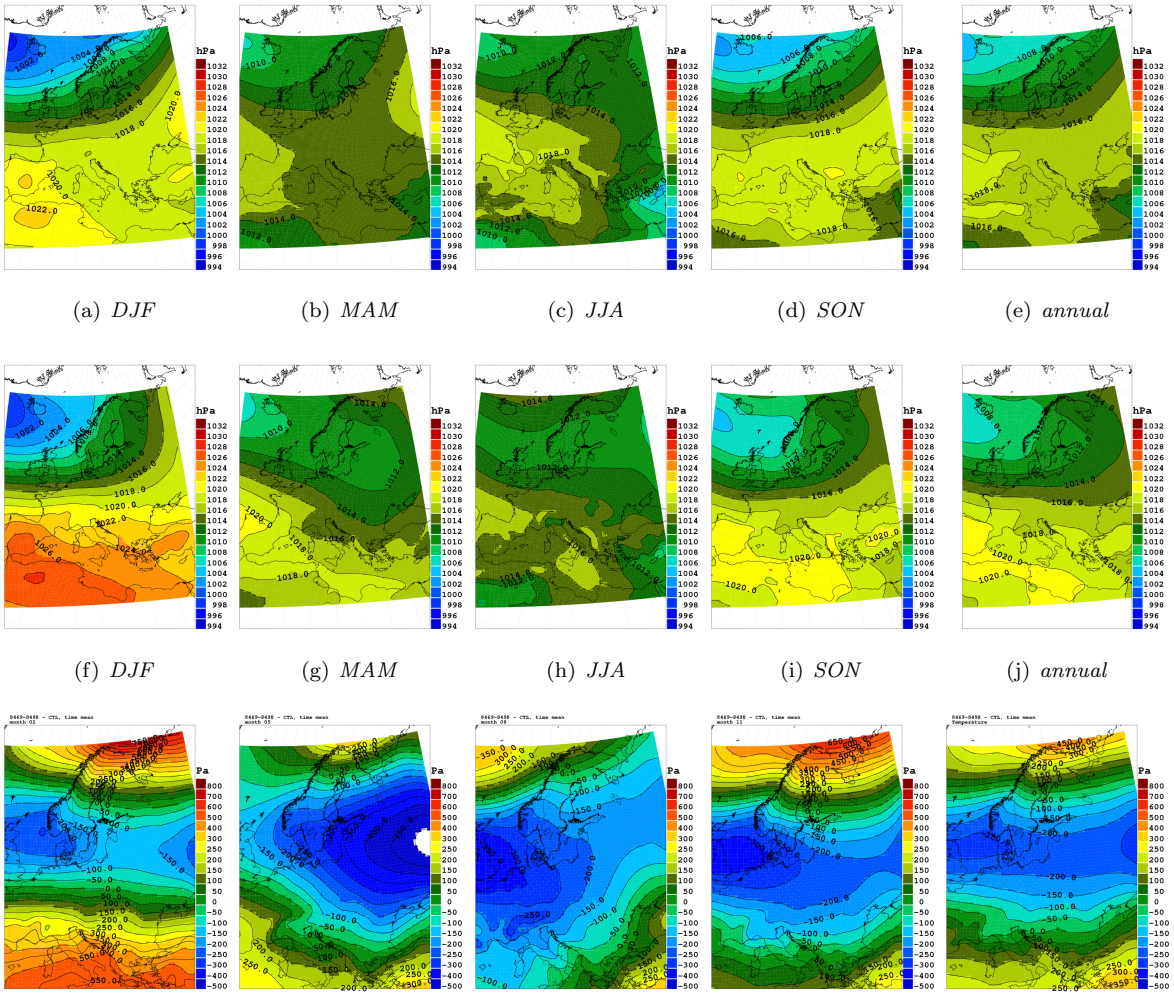

(a) *DJF* (b) *MAM* (c) *JJA* (d) *SON* (e) *annual*

(f) *DJF* (g) *MAM* (h) *JJA* (i) *SON* (j) *annual*

(k) *DJF* (l) *MAM* (m) *JJA* (n) *SON* (o) *annual*

Figure 4. The long term mean of the SLP in the RCA3 control run forced with ERA40 for the period Dec. 1968 until Nov. 1998 (top row), the corresponding period in the simulation forced with ECHO-G (middle), and the differences between both. Single rows include seasonal (DJF, MAM, JJA and SON) and annual means (from left to right).

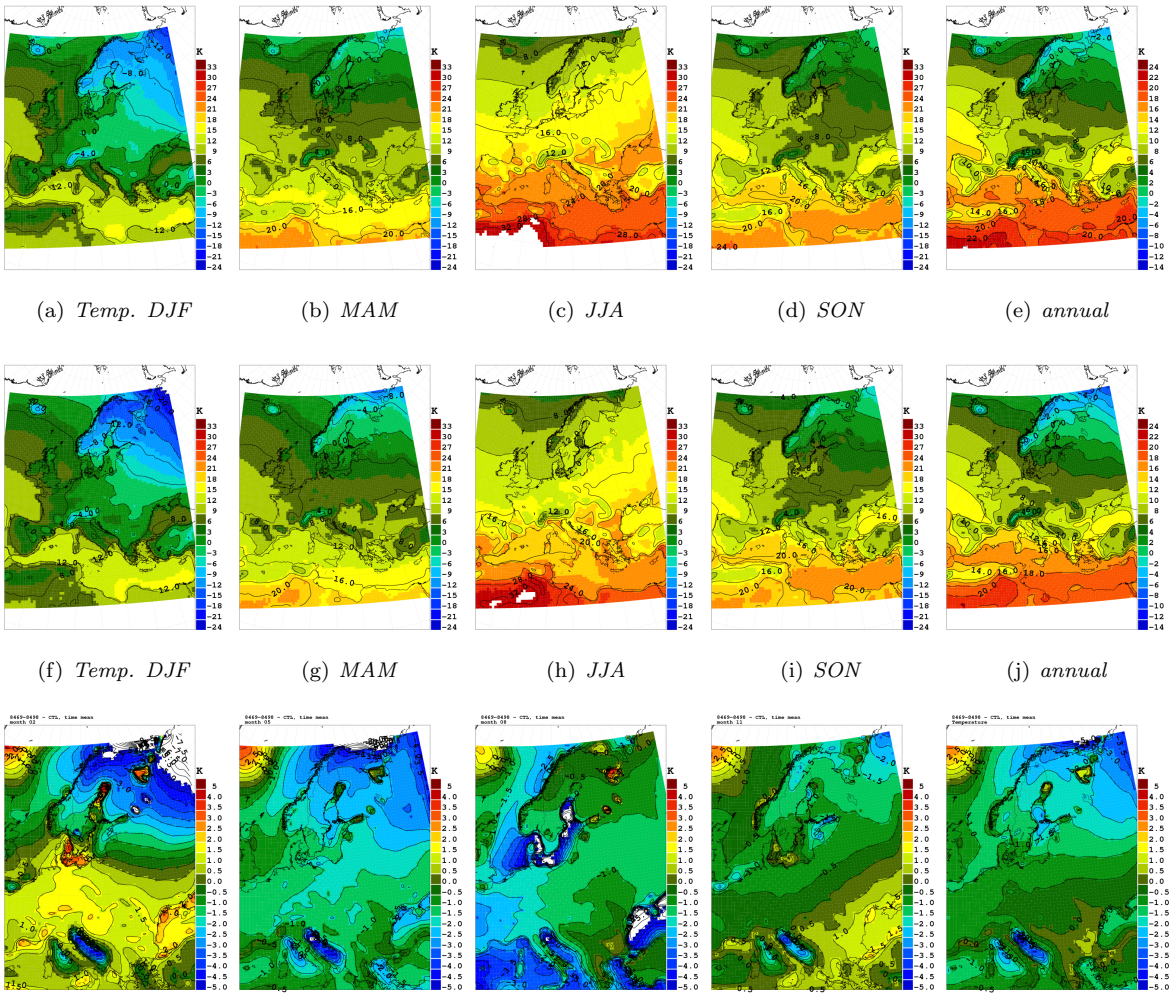

(a) *Temp. DJF* (b) *MAM* (c) *JJA* (d) *SON* (e) *annual*

(f) *Temp. DJF* (g) *MAM* (h) *JJA* (i) *SON* (j) *annual*

(k) *Temp. DJF* (l) *MAM* (m) *JJA* (n) *SON* (o) *annual*

Figure 5. Same as Fig. 4 only for the 2m air temperature.

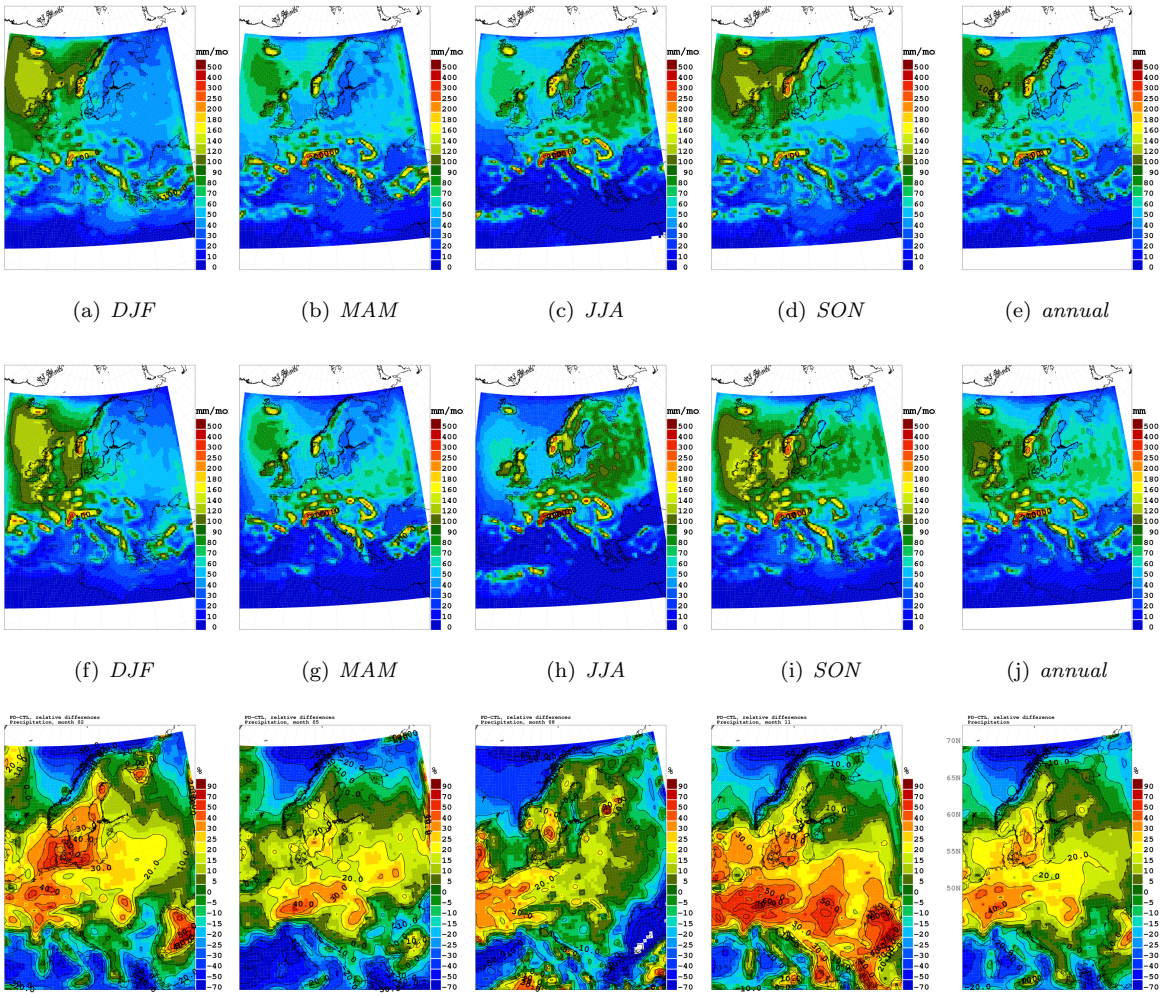

(a) *DJF* (b) *MAM* (c) *JJA* (d) *SON* (e) *annual*

(f) *DJF* (g) *MAM* (h) *JJA* (i) *SON* (j) *annual*

(k) *DJF* (l) *MAM* (m) *JJA* (n) *SON* (o) *annual*

Figure 6. Same as Fig. 4 only for precipitation.

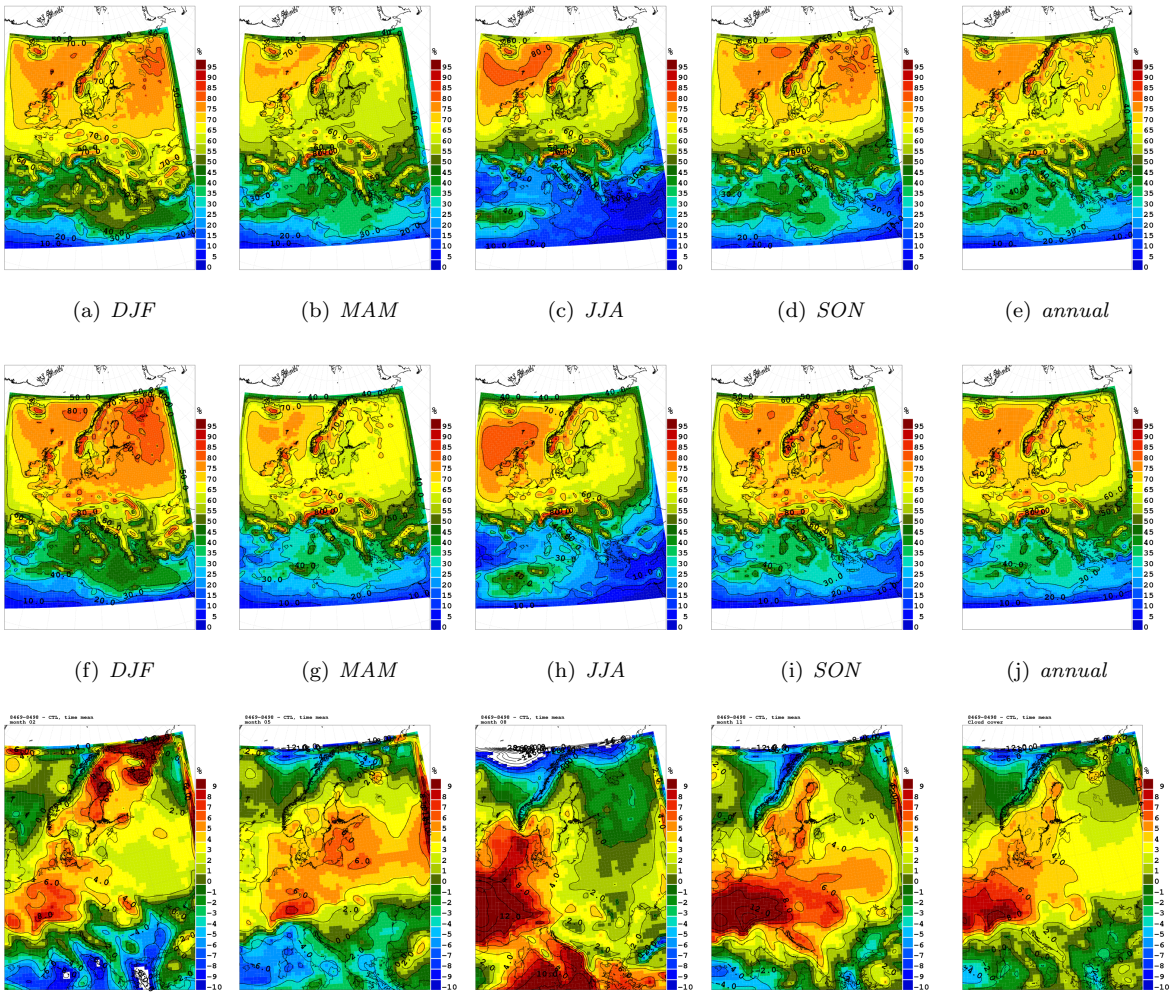

(a) *DJF* (b) *MAM* (c) *JJA* (d) *SON* (e) *annual*

(f) *DJF* (g) *MAM* (h) *JJA* (i) *SON* (j) *annual*

(k) *DJF* (l) *MAM* (m) *JJA* (n) *SON* (o) *annual*

Figure 7. Same as Fig. 4 only for cloud cover.

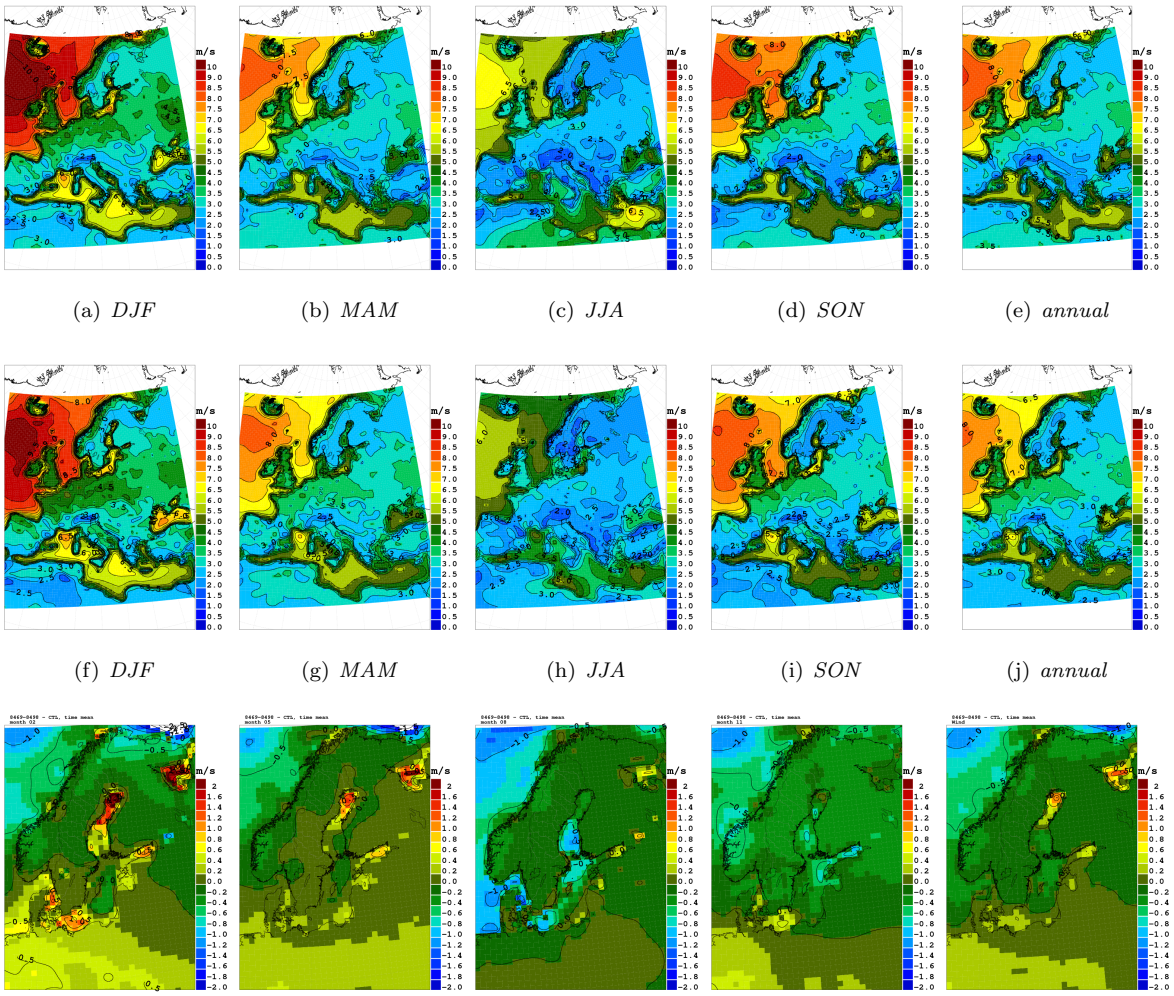

(a) *DJF* (b) *MAM* (c) *JJA* (d) *SON* (e) *annual*

(f) *DJF* (g) *MAM* (h) *JJA* (i) *SON* (j) *annual*

(k) *DJF* (l) *MAM* (m) *JJA* (n) *SON* (o) *annual*

Figure 8. Same as Fig. 4 only for 10m wind speed.

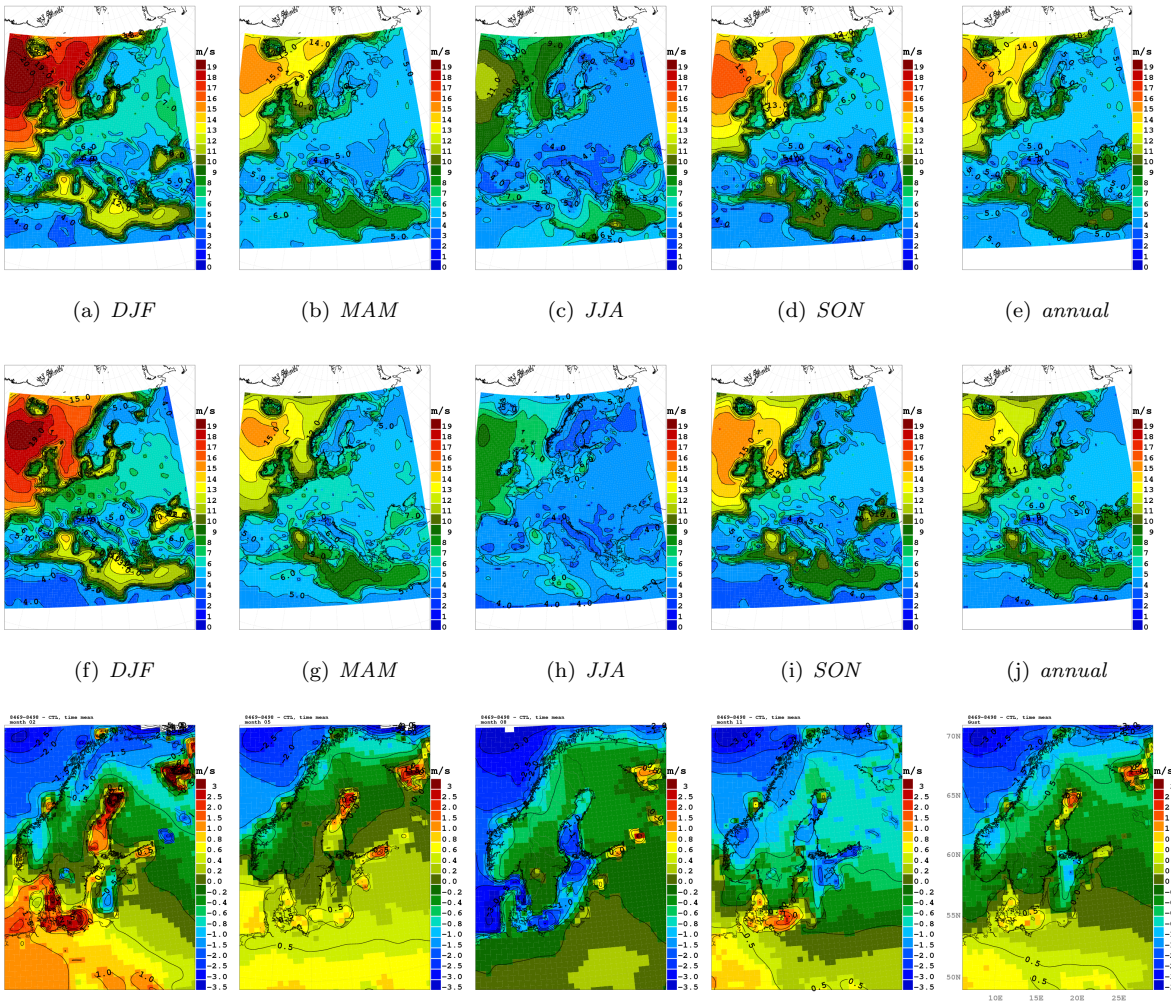

(a) *DJF* (b) *MAM* (c) *JJA* (d) *SON* (e) *annual*

(f) *DJF* (g) *MAM* (h) *JJA* (i) *SON* (j) *annual*

(k) *DJF* (l) *MAM* (m) *JJA* (n) *SON* (o) *annual*

Figure 9. Same as Fig. 4 only for the gustiness.

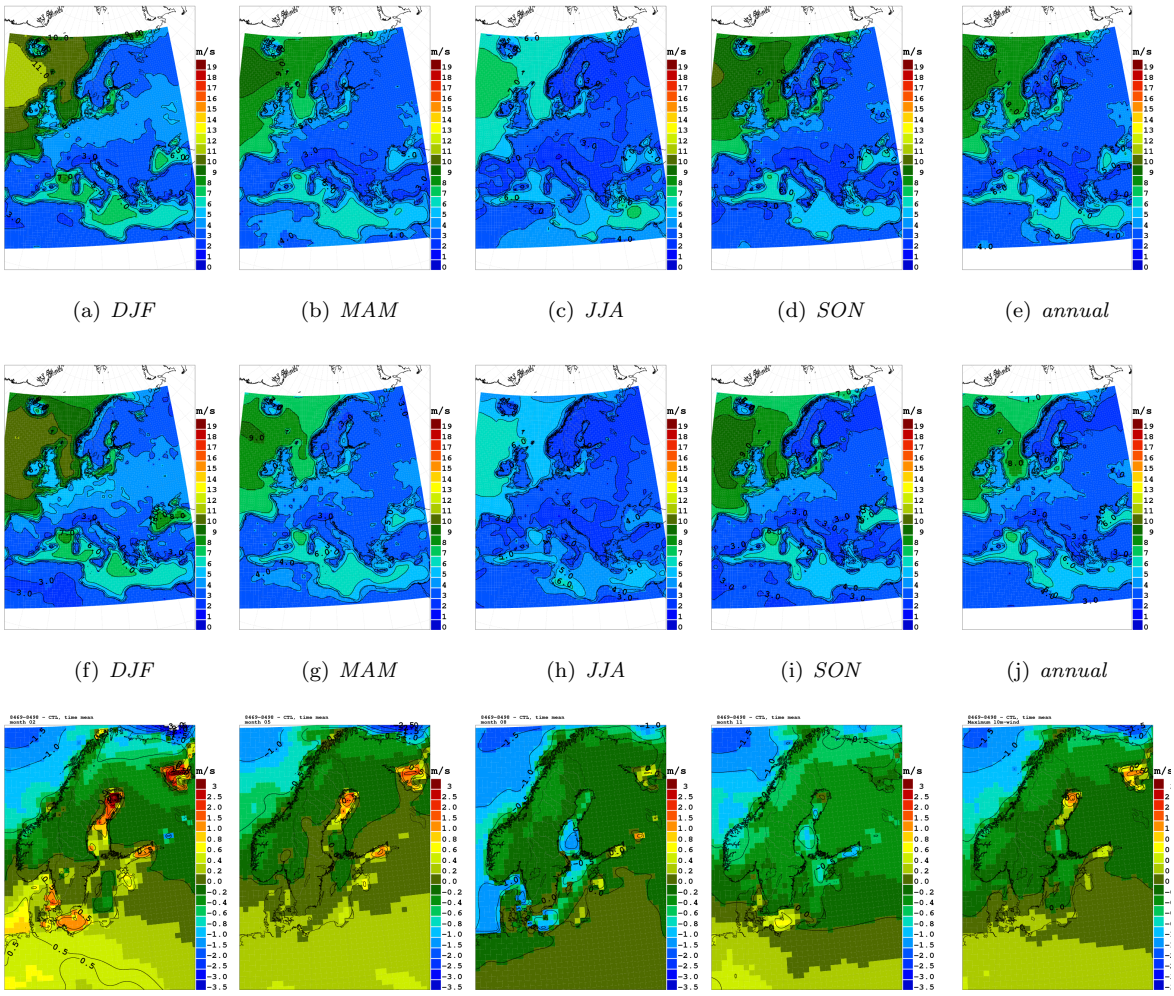

(a) *DJF* (b) *MAM* (c) *JJA* (d) *SON* (e) *annual*

(f) *DJF* (g) *MAM* (h) *JJA* (i) *SON* (j) *annual*

(k) *DJF* (l) *MAM* (m) *JJA* (n) *SON* (o) *annual*

Figure 10. Same as Fig. 4 only for the maximum 10m wind speed.

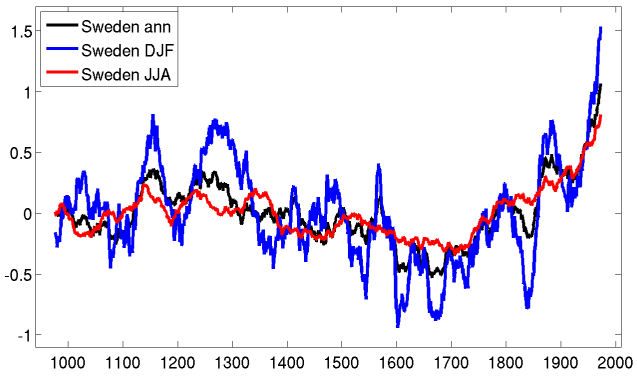

(a) *DJF and JJA*

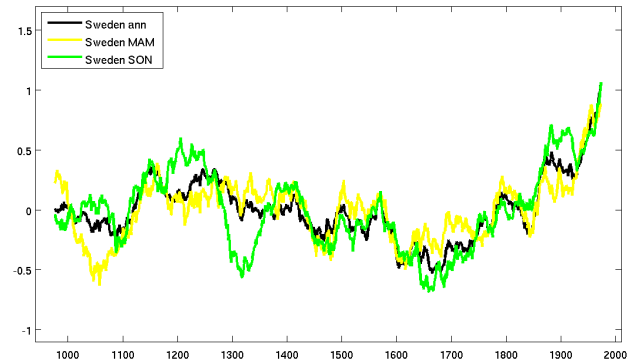

(b) *MAM and SON*

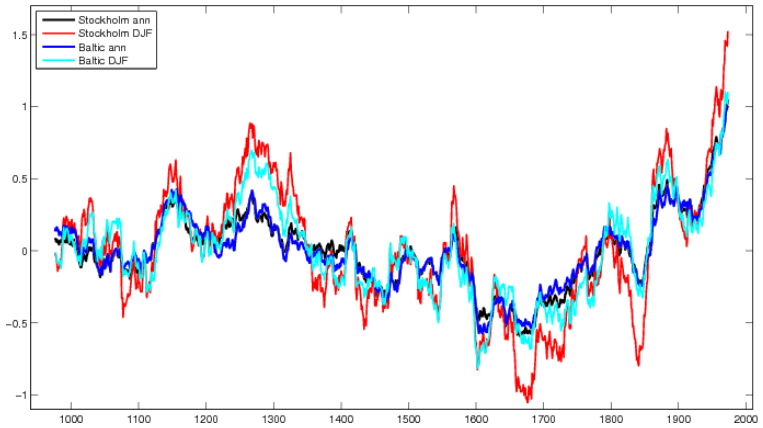

(c) *Stockholm and Baltic*

Figure 11. Temporal evolution of temperatures in the simulation for different seasons and regions. Annual, winter and summer mean temperature over Sweden (a) as well as annual, spring and autumn (b). c) Temperatures for a single grid-box close to Stockholm and over the Baltic Sea (east of Gotland).

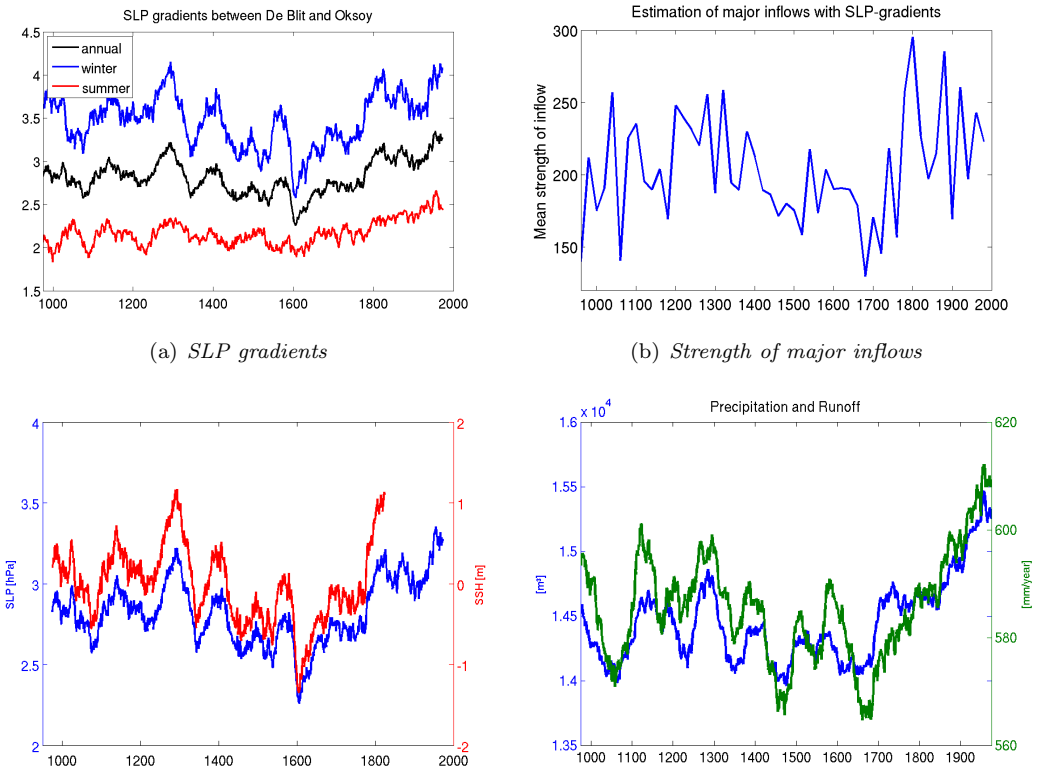

(a) *SLP gradients* (b) *Strength of major inflows*

(c) *SLP and SSH* (d) *Precipitation and Runoff*

Figure 12. 50-year running means of SLP gradients between De Blit (Netherlands) and Oksøy (Norway) for DJF, JJA and annual means (a), the estimated strength of inflows based on SLP gradients accumulated over 20-year periods (b), the annual SLP gradient and the related sea surface height (SSH) (c), and the mean precipitation in combination with the computed runoff into the Baltic Sea as annual means (d).

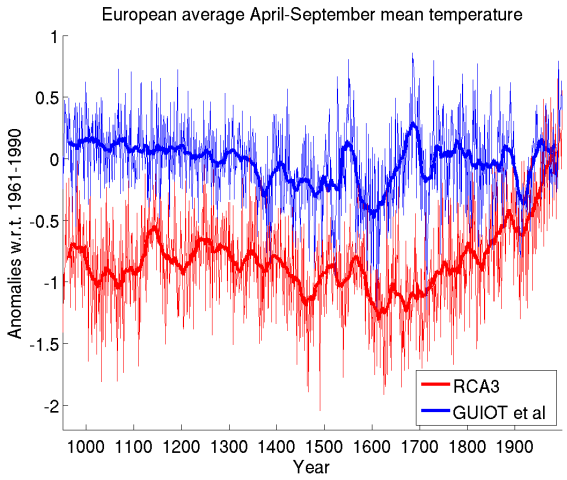

(a)

Figure 13. Multi-proxy reconstruction of the European average April-September mean temperature anomalies from *Guiot et al.* [2010] and the corresponding simulated temperatures from RCA3. The thin lines show data for each year while the thick lines show 30-year running means.

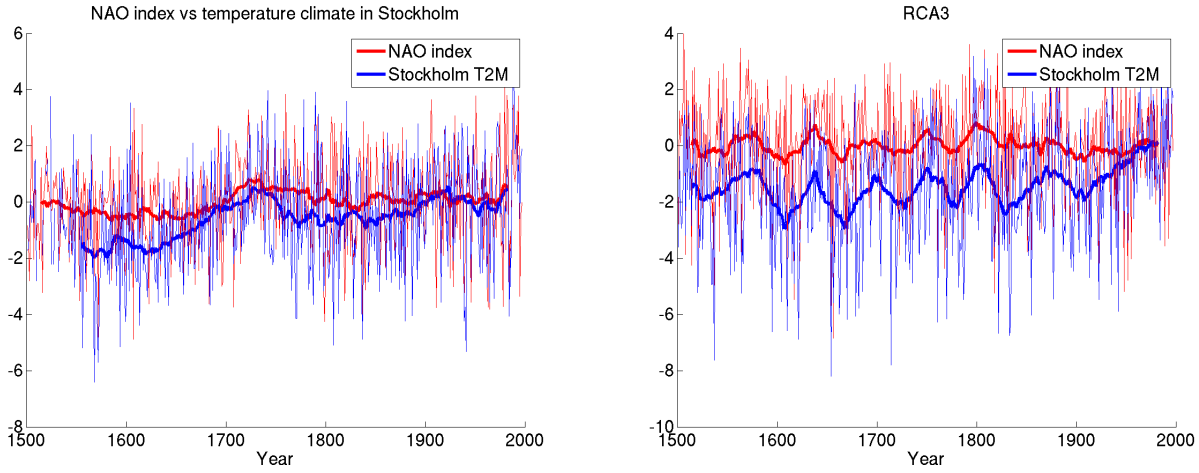

(a) (b)

Figure 14. a) Proxy-based reconstruction of the NAO index representing December-February [*Luterbacher et al.*, 2002] and proxy-based estimates of January-April Stockholm mean temperature anomalies w.r.t to the long-term average [*Leijonhufvud et al.*, 2009]. The thin lines show data for each year while the thick lines show 30-year running means. b) Model-derived NAO index for Stockholm mean December-February and January-April temperature anomalies w.r.t. the long-term average. The thin lines show data for each year while the thick lines show 30-year running means.

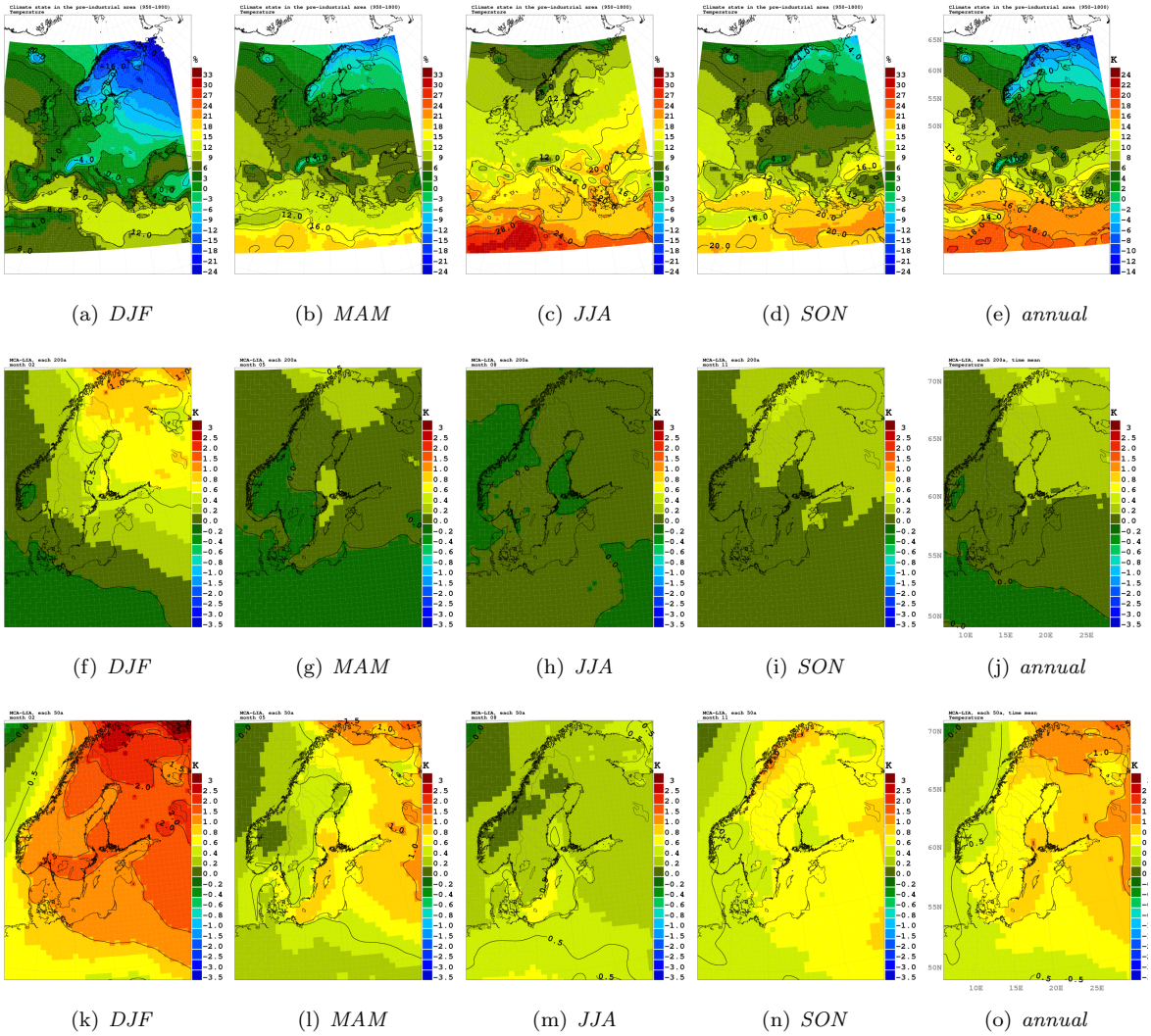

(a) *DJF* (b) *MAM* (c) *JJA* (d) *SON* (e) *annual*

(f) *DJF* (g) *MAM* (h) *JJA* (i) *SON* (j) *annual*

(k) *DJF* (l) *MAM* (m) *JJA* (n) *SON* (o) *annual*

Figure 15. The mean temperature in the pre-industrial control state (950-1800) (top). (middle) MCA minus LIA for the 200 year periods. (bottom) Temperature differences between the 50 warmest years of MCA (1246-1295) and the 50 coldest years of LIA (1647-1696). Single rows include seasonal (DJF, MAM, JJA and SON) and annual means (from left to right).

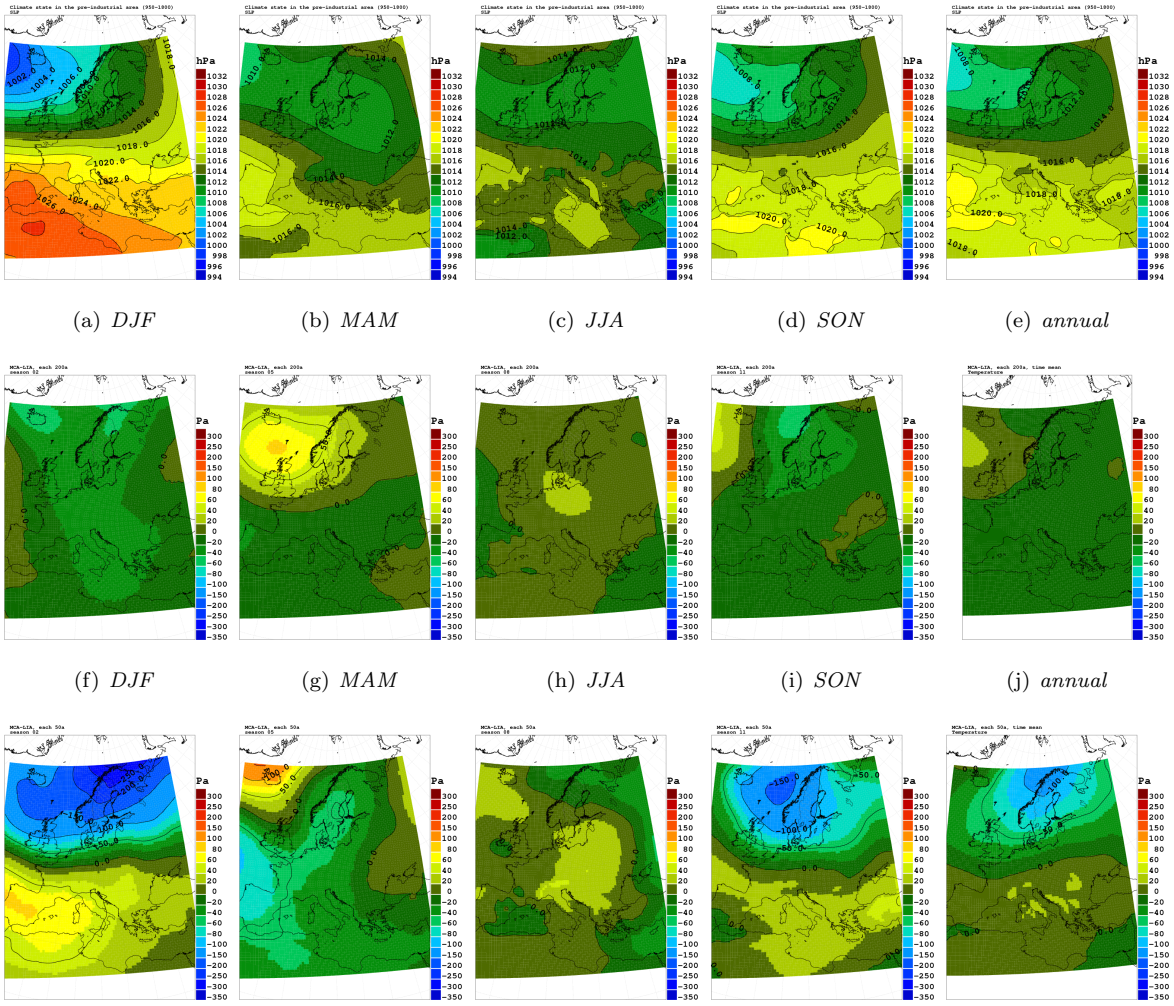

(a) *DJF* (b) *MAM* (c) *JJA* (d) *SON* (e) *annual*

(f) *DJF* (g) *MAM* (h) *JJA* (i) *SON* (j) *annual*

(k) *DJF* (l) *MAM* (m) *JJA* (n) *SON* (o) *annual*

Figure 16. (top) The SLP mean fields during the pre-industrial control period (950-1800). (middle) SLP differences between the full 200 years periods of MCA and LIA. (bottom) SLP differences between the 50 warmest years of MCA (1246-1295) and the 50 coldest years of LIA (1647-1696). Single rows include seasonal (DJF, MAM, JJA and SON) and annual means (from left to right).

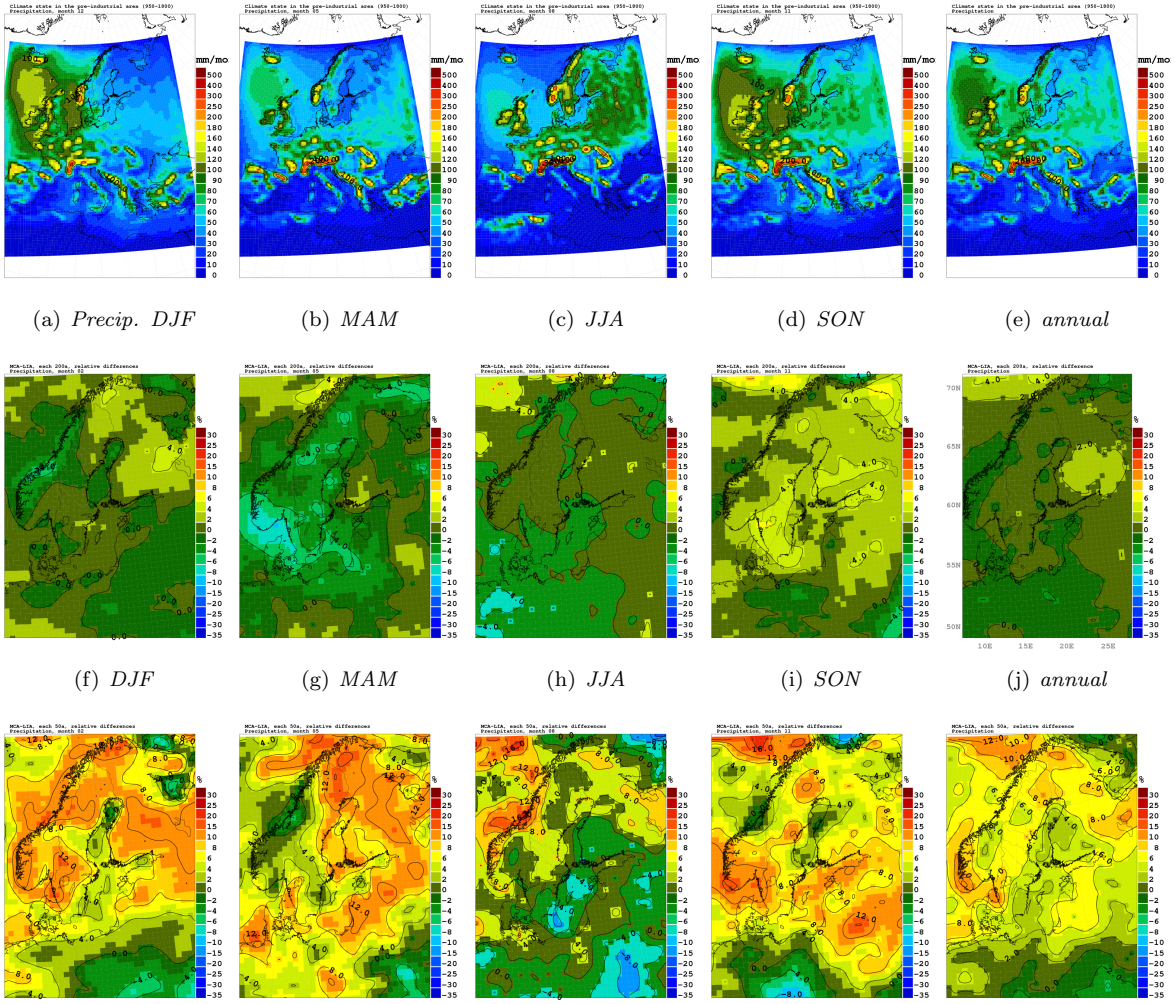

(a) *Precip. DJF* (b) *MAM* (c) *JJA* (d) *SON* (e) *annual*

(f) *DJF* (g) *MAM* (h) *JJA* (i) *SON* (j) *annual*

(k) *DJF* (l) *MAM* (m) *JJA* (n) *SON* (o) *annual*

Figure 17. Same as Fig. 16 only for precipitation. Note that the absolute values are given in mm/month whereas the differences between MCA and LIA are shown as percentages.

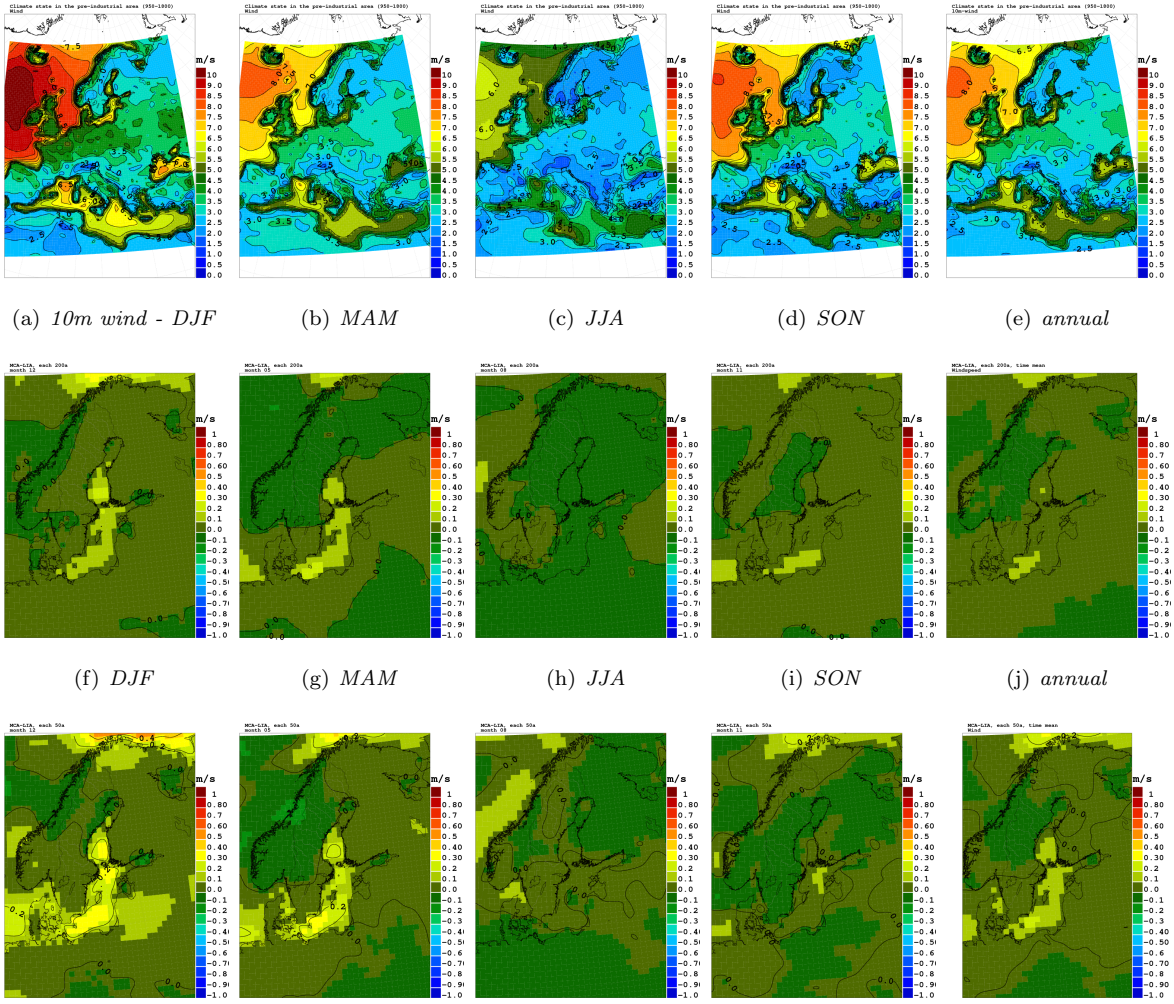

(a) *10m wind - DJF* (b) *MAM* (c) *JJA* (d) *SON* (e) *annual*

(f) *DJF* (g) *MAM* (h) *JJA* (i) *SON* (j) *annual*

(k) *DJF* (l) *MAM* (m) *JJA* (n) *SON* (o) *annual*

Figure 18. Same as Fig. 16 only for 10m wind speed.

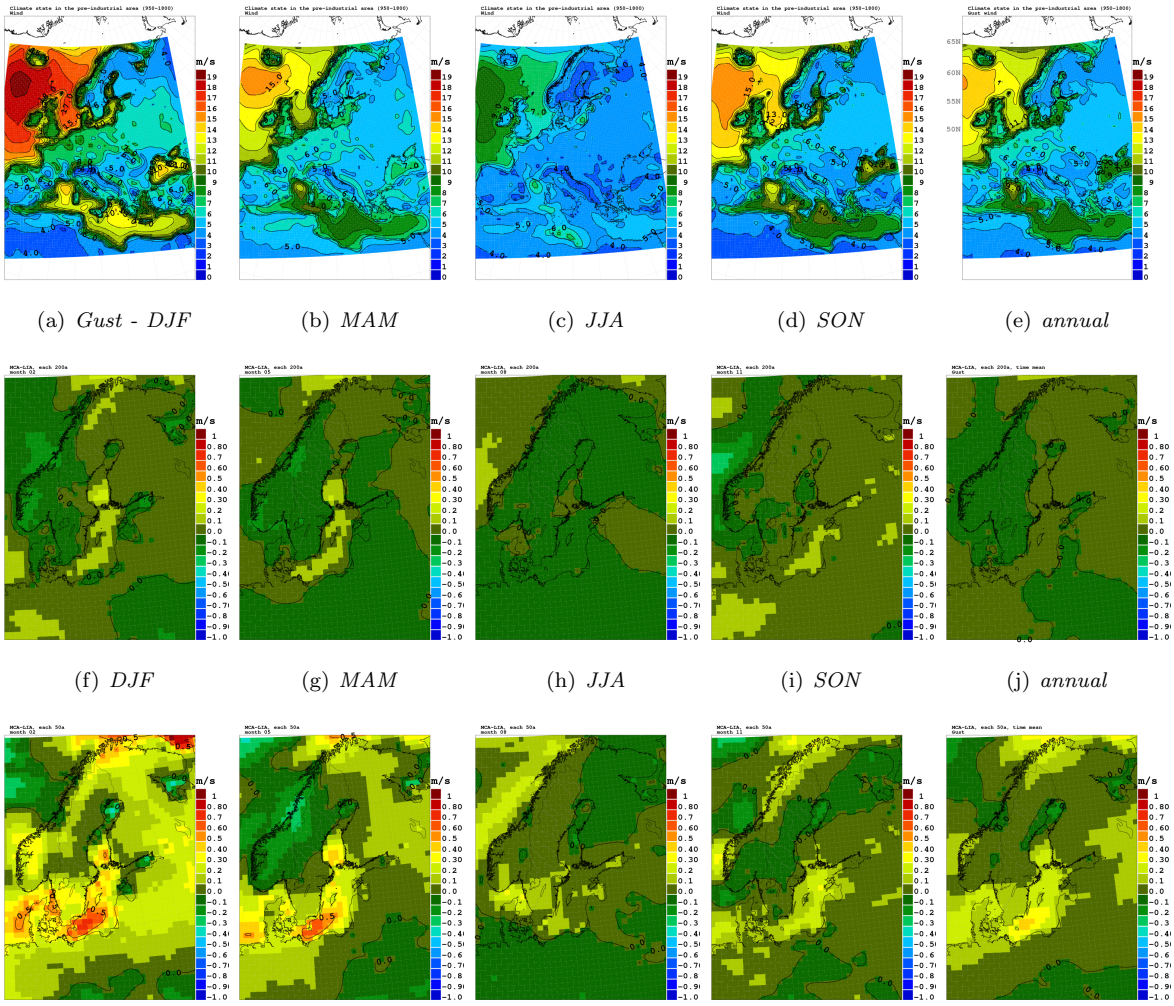

(a) *Gust - DJF* (b) *MAM* (c) *JJA* (d) *SON* (e) *annual*

(f) *DJF* (g) *MAM* (h) *JJA* (i) *SON* (j) *annual*

(k) *DJF* (l) *MAM* (m) *JJA* (n) *SON* (o) *annual*

Figure 19. Same as Fig. 16 only for gustiness.

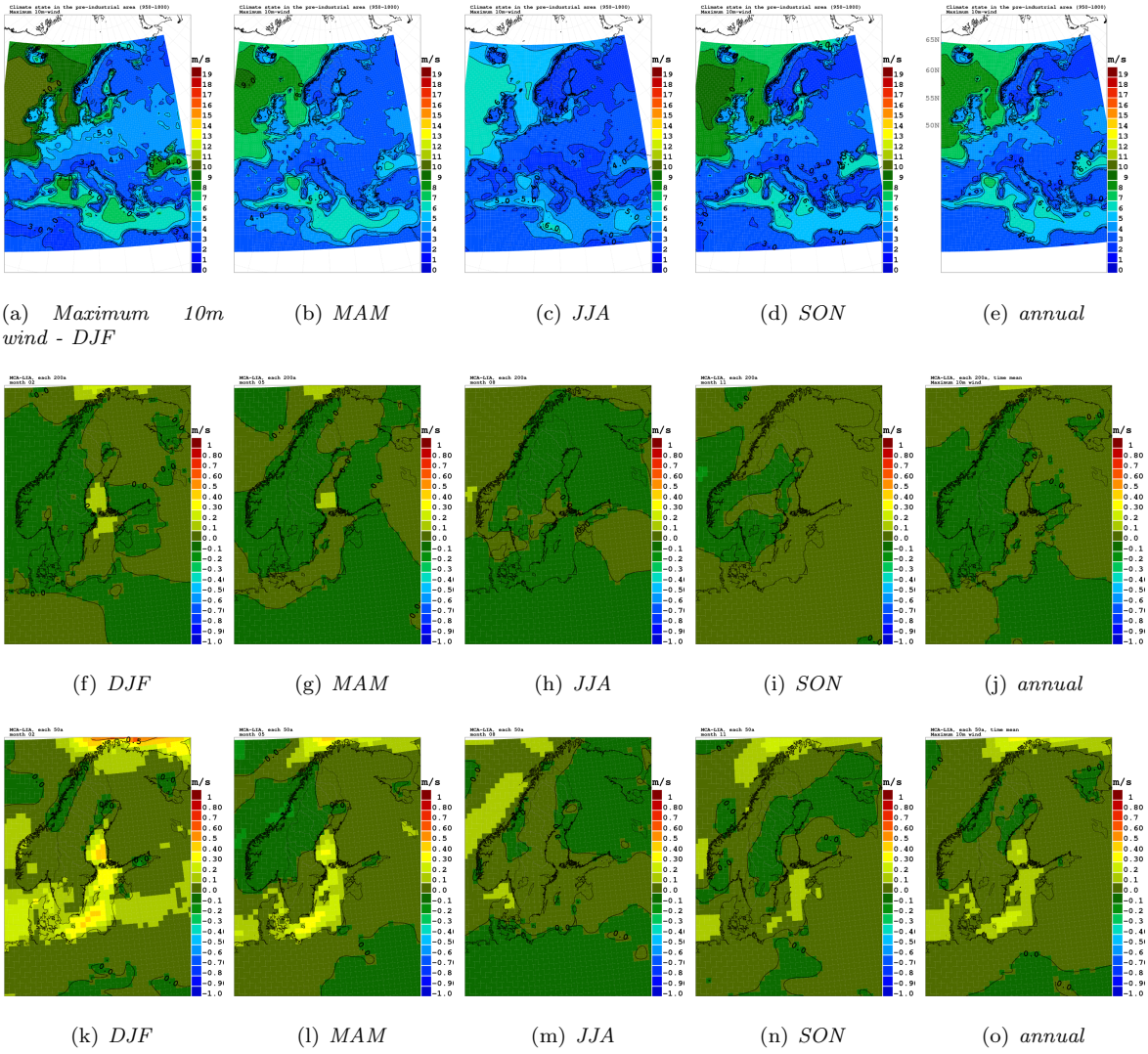

(a) *Maximum 10m wind - DJF* (b) *MAM* (c) *JJA* (d) *SON* (e) *annual*

(f) *DJF* (g) *MAM* (h) *JJA* (i) *SON* (j) *annual*

(k) *DJF* (l) *MAM* (m) *JJA* (n) *SON* (o) *annual*

Figure 20. Same as Fig. 16 only for the maximum 10m wind speed.

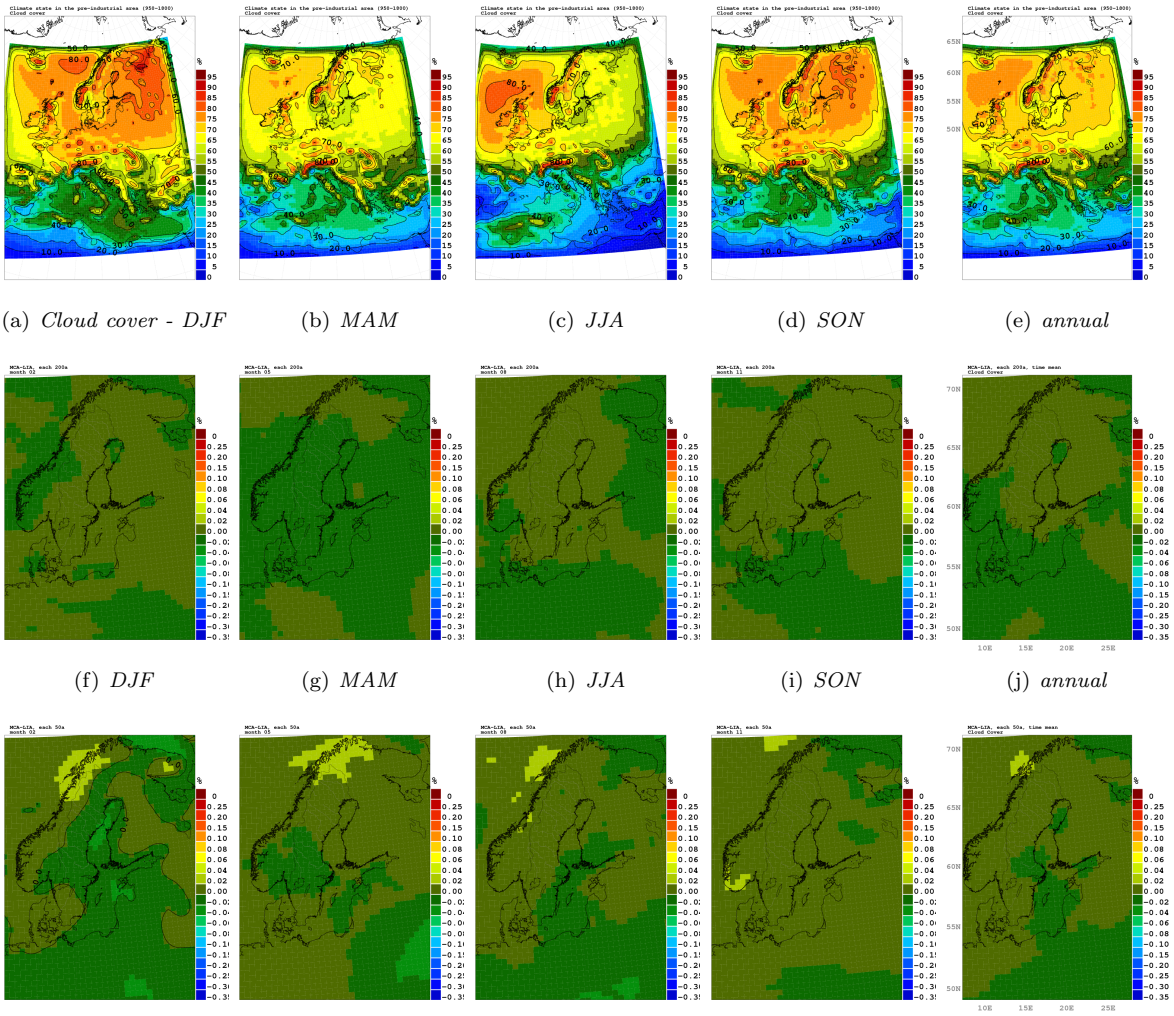

(a) *Cloud cover - DJF* (b) *MAM* (c) *JJA* (d) *SON* (e) *annual*

(f) *DJF* (g) *MAM* (h) *JJA* (i) *SON* (j) *annual*

(k) *DJF* (l) *MAM* (m) *JJA* (n) *SON* (o) *annual*

Figure 21. Same as Fig. 16 only for cloud cover.

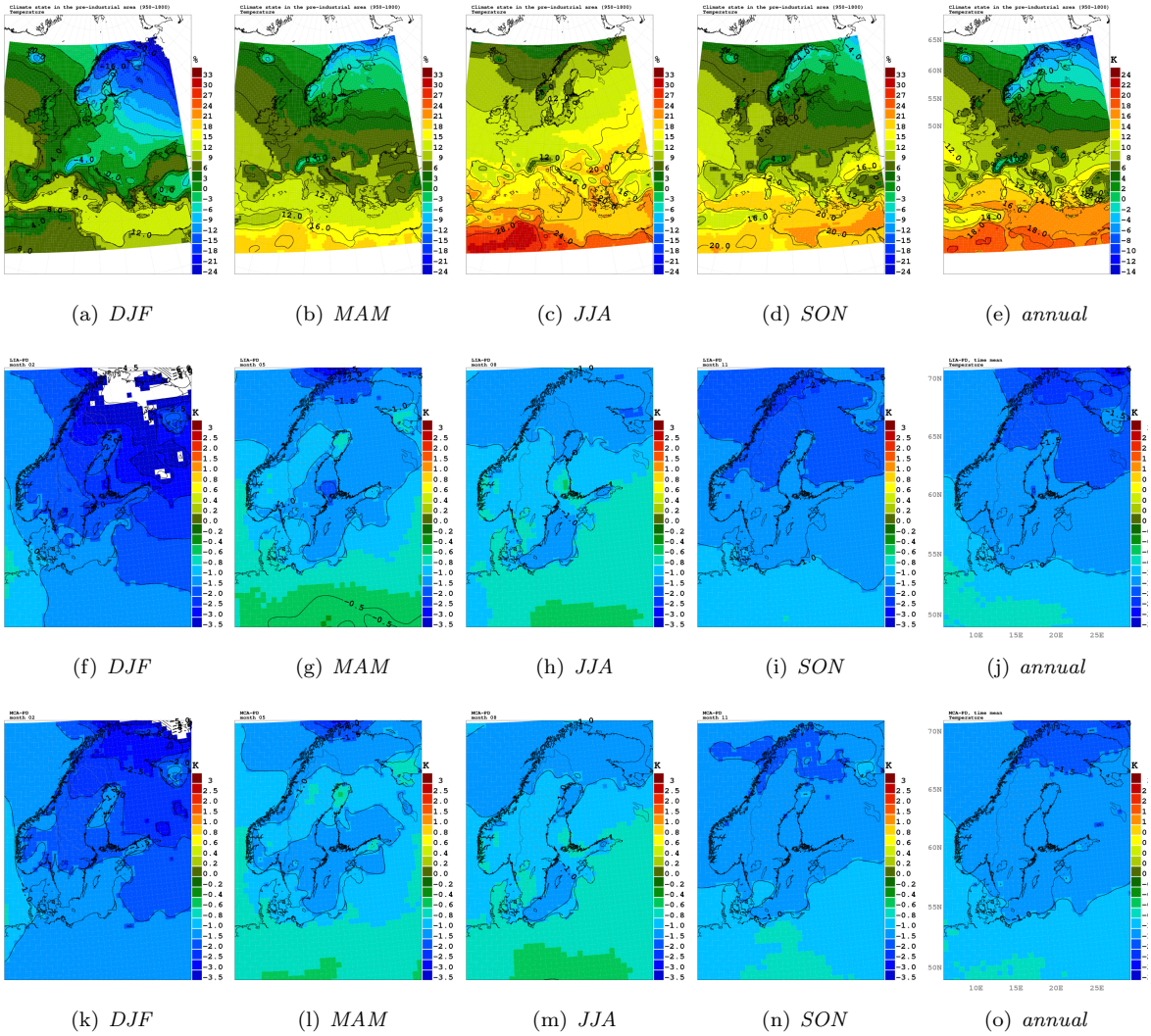

(a) *DJF* (b) *MAM* (c) *JJA* (d) *SON* (e) *annual*

(f) *DJF* (g) *MAM* (h) *JJA* (i) *SON* (j) *annual*

(k) *DJF* (l) *MAM* (m) *JJA* (n) *SON* (o) *annual*

Figure 22. The mean temperature in the pre-industrial control state (top). Temperature signals for LIA minus present day climate taken from the simulation forced with ECHO-G (second row). (third row) MCA compared to the present day climate. Single rows include seasonal (DJF, MAM, JJA and SON) and annual means (from left to right).

I serien OCEANOGRAFI har tidigare utgivits:

1 Lennart Funkquist (1985)
En hydrodynamisk modell för spridnings- och cirkulationsberäkningar i Östersjön Slutrapport.

2 Barry Broman och Carsten Pettersson. (1985)
Spridningsundersökningar i yttre fjärden Piteå.

3 Cecilia Ambjörn (1986).
Utbyggnad vid Malmö hamn; effekter för Lommabuktens vattenutbyte.

4 Jan Andersson och Robert Hillgren (1986).
SMHIs undersökningar i Öregrundsgrepen perioden 84/85.

5 Bo Juhlin (1986)
Oceanografiska observationer utmed svenska kusten med kustbevakningens fartyg 1985.

6 Barry Broman (1986)
Uppföljning av sjövärmepump i Lilla Värtan.

7 Bo Juhlin (1986)
15 års mätningar längs svenska kusten med kustbevakningen (1970 - 1985).

8 Jonny Svensson (1986)
Vågdata från svenska kustvatten 1985.

9 Barry Broman (1986)
Oceanografiska stationsnät - Svenskt Vattenarkiv.

10 -

11 Cecilia Ambjörn (1987)
Spridning av kylvatten från Öresundsverket

12 Bo Juhlin (1987)
Oceanografiska observationer utmed svenska kusten med kustbevakningens fartyg 1986.

13 Jan Andersson och Robert Hillgren (1987)
SMHIs undersökningar i Öregrundsgrepen 1986.

14 Jan-Erik Lundqvist (1987)
Impact of ice on Swedish offshore lighthouses. Ice drift conditions in the area at Sydostbrotten - ice season 1986/87.

15 SMHI/SNV (1987)
Fasta förbindelser över Öresund - utredning av effekter på vattenmiljön i Östersjön.

16 Cecilia Ambjörn och Kjell Wickström (1987)
Undersökning av vattenmiljön vid utfyllnaden av Kockums varvsbassäng. Slutrapport för perioden
18 juni - 21 augusti 1987.

17 Erland Bergstrand (1987)
Östergötlands skärgård - Vattenmiljön.

18 Stig H. Fonselius (1987)
Kattegatt - havet i väster.

19 Erland Bergstrand (1987)
Recipientkontroll vid Breviksnäs fiskodling 1986.

20 Kjell Wickström (1987)
Bedömning av kylvattenrecipienten för ett kolkraftverk vid Oskarshamnsverket.

21 Cecilia Ambjörn (1987)
Förstudie av ett nordiskt modellsystem för kemikaliespridning i vatten.

22 Kjell Wickström (1988)
Vågdata från svenska kustvatten 1986.

23 Jonny Svensson, SMHI/National Swedish Environmental Protection Board (SNV) (1988)
A permanent traffic link across the Öresund channel - A study of the hydro-environmental effects in the Baltic Sea.

24 Jan Andersson och Robert Hillgren (1988)
SMHIs undersökningar utanför Forsmark 1987.

25 Carsten Peterson och Per-Olof Skoglund (1988)
Kylvattnet från Ringhals 1974-86.

26 Bo Juhlin (1988)
Oceanografiska observationer runt svenska kusten med kustbevakningens fartyg 1987.

27 Bo Juhlin och Stefan Tobiasson (1988)
Recipientkontroll vid Breviksnäs fiskodling 1987.

28 Cecilia Ambjörn (1989)
Spridning och sedimentation av tippat lermaterial utanför Helsingborgs hamnområde.

29 Robert Hillgren (1989)
SMHIs undersökningar utanför Forsmark 1988.

30 Bo Juhlin (1989)
Oceanografiska observationer runt svenska kusten med kustbevakningens fartyg 1988.

31 Erland Bergstrand och Stefan Tobiasson (1989)
Samordnade kustvattenkontrollen i Östergötland 1988.

32 Cecilia Ambjörn (1989)
Oceanografiska förhållanden i Brofjorden i samband med kylvattenutsläpp i Trommekilen.

33a Cecilia Ambjörn (1990)
Oceanografiska förhållanden utanför Vendelsöfjorden i samband med kylvatten-utsläpp.

33b Eleonor Marmefelt och Jonny Svensson (1990)
Numerical circulation models for the Skagerrak - Kattegat. Preparatory study.

34 Kjell Wickström (1990)
Oskarshamnsverket - kylvattenutsläpp i havet - slutrapport.

35 Bo Juhlin (1990)
Oceanografiska observationer runt svenska kusten med kustbevakningens fartyg 1989.

36 Bertil Håkansson och Mats Moberg (1990)
Glommaälvens spridningsområde i nord-östra Skagerrak

37 Robert Hillgren (1990)
SMHIs undersökningar utanför Forsmark 1989.

38 Stig Fonselius (1990)
Skagerrak - the gateway to the North Sea.

39 Stig Fonselius (1990)
Skagerrak - porten mot Nordsjön.

40 Cecilia Ambjörn och Kjell Wickström (1990)
Spridningsundersökningar i norra Kalmarsund för Mönsterås bruk.

41 Cecilia Ambjörn (1990)
Strömningsteknisk utredning avseende utbyggnad av gipsdeponi i Landskrona.

42 Cecilia Ambjörn, Torbjörn Grafström och Jan Andersson (1990)
Spridningsberäkningar - Klints Bank.

43 Kjell Wickström och Robert Hillgren (1990)
Spridningsberäkningar för EKA-NOBELs fabrik i Stockviksverken.

44 Jan Andersson (1990)
Brofjordens kraftstation - Kylvattenspridning i Hanneviken.

45 Gustaf Westring och Kjell Wickström (1990)
Spridningsberäkningar för Höganäs kommun.

46 Robert Hillgren och Jan Andersson (1991)
SMHIs undersökningar utanför Forsmark 1990.

47 Gustaf Westring (1991)
Brofjordens kraftstation - Kompletterande simulering och analys av kylvattenspridning i Trommekilen.

48 Gustaf Westring (1991)
Vågmätningar utanför Kristianopel - Slutrapport.

49 Bo Juhlin (1991)
Oceanografiska observationer runt svenska kusten med kustbevakningens fartyg 1990.

50A Robert Hillgren och Jan Andersson (1992)
SMHIs undersökningar utanför Forsmark 1991.

50B Thomas Thompson, Lars Ulander, Bertil Håkansson, Bertil Brusmark, Anders Carlström, Anders Gustavsson, Eva Cronström och Olov Fäst (1992).
BEERS -92. Final edition.

51 Bo Juhlin (1992)
Oceanografiska observationer runt svenska kusten med kustbevakningens fartyg 1991.

52 Jonny Svensson och Sture Lindahl (1992)
Numerical circulation model for the Skagerrak - Kattegat.

53 Cecilia Ambjörn (1992)
Isproppsförebyggande muddring och dess inverkan på strömmarna i Torneälven.

54 Bo Juhlin (1992)
20 års mätningar längs svenska kusten med kustbevakningens fartyg (1970 - 1990).

55 Jan Andersson, Robert Hillgren och Gustaf Westring (1992)
Förstudie av strömmar, tidvatten och vattenstånd mellan Cebu och Leyte, Filippinerna.

56 Gustaf Westring, Jan Andersson, Henrik Lindh och Robert Axelsson (1993)
Forsmark - en temperaturstudie.
Slutrapport.

57 Robert Hillgren och Jan Andersson (1993)
SMHIs undersökningar utanför Forsmark 1992.

58 Bo Juhlin (1993)
Oceanografiska observationer runt svenska kusten med kustbevakningens fartyg 1992.

59 Gustaf Westring (1993)
Isförhållandena i svenska farvatten under normalperioden 1961-90.

60 Torbjörn Lindkvist (1994)
Havsområdesregister 1993.

61 Jan Andersson och Robert Hillgren (1994)
SMHIs undersökningar utanför Forsmark 1993.

62 Bo Juhlin (1994)
Oceanografiska observationer runt svenska kusten med kustbevakningens fartyg 1993.

63 Gustaf Westring (1995)
Isförhållanden utmed Sveriges kust - isstatistik från svenska farleder och farvatten under normalperioderna 1931-60 och 1961-90.

64 Jan Andersson och Robert Hillgren (1995)
SMHIs undersökningar utanför Forsmark 1994.

65 Bo Juhlin (1995)
Oceanografiska observationer runt svenska kusten med kustbevakningens fartyg 1994.

66 Jan Andersson och Robert Hillgren (1996)
SMHIs undersökningar utanför Forsmark 1995.

67 Lennart Funkquist och Patrik Ljungemyr (1997)
Validation of HIROMB during 1995-96.

68 Maja Brandt, Lars Edler och Lars Andersson (1998)
Översvämningar längs Oder och Wisla sommaren 1997 samt effekterna i Östersjön.

69 Jörgen Sahlberg SMHI och Håkan Olsson, Länsstyrelsen, Östergötland (2000).
Kustzonsmodell för norra Östergötlands skärgård.

70 Barry Broman (2001)
En vågatlas för svenska farvatten.
Ej publicerad

71 ***Vakant – kommer ej att utnyttjas!***

72 Fourth Workshop on Baltic Sea Ice Climate
Norrköping, Sweden 22-24 May, 2002
Conference Proceedings
Editors: Anders Omstedt and Lars Axell

73 Torbjörn Lindkvist, Daniel Björkert, Jenny Andersson, Anders Gyllander (2003)
Djupdata för havsområden 2003

74 Håkan Olsson, SMHI (2003)
Erik Årnefelt, Länsstyrelsen Östergötland
Kustzonssystemet i regional miljöanalys

75 Jonny Svensson och Eleonor Marmefelt (2003)
Utvärdering av kustzonsmodellen för norra Östergötlands och norra Bohusläns skärgårdar

76 Eleonor Marmefelt, Håkan Olsson, Helma Lindow och Jonny Svensson, Thalassos Computations (2004)
Integrerat kustzonssystem för Bohusläns skärgård

77 Philip Axe, Martin Hansson och Bertil Håkansson (2004)
The national monitoring programme in the Kattegat and Skagerrak

78 Lars Andersson, Nils Kajrup och Björn Sjöberg (2004)
Dimensionering av det nationella marina pelagialprogrammet

79 Jörgen Sahlberg (2005)
Randdata från öppet hav till kustzons-modellerna (Exemplet södra Östergötland)

80 Eleonor Marmefelt, Håkan Olsson (2005)
Integrerat Kustzonssystem för Hallandskusten

81 Tobias Strömgren (2005)
Implementation of a Flux Corrected Transport scheme in the Rossby Centre Ocean model

82 Martin Hansson (2006)
Cyanobakterieblomningar i Östersjön, resultat från satellitövervakning 1997-2005

83 Kari Eilola, Jörgen Sahlberg (2006)
Model assessment of the predicted environmental consequences for OSPAR problem areas following nutrient reductions

84 Torbjörn Lindkvist, Helma Lindow (2006)
Fyrskeppsdata. Resultat och bearbetnings-metoder med exempel från Svenska Björn 1883 – 1892

85 Pia Andersson (2007)
Ballast Water Exchange areas – Prospect of designating BWE areas in the Baltic Proper

86 Elin Almroth, Kari Eilola, M. Skogen, H. Søiland and Ian Sehested Hansen (2007)
The year 2005. An environmental status report of the Skagerrak, Kattegat and North Sea

87 Eleonor Marmefelt, Jörgen Sahlberg och Marie Bergstrand (2007)
HOME Vatten i södra Östersjöns vattendistrikt. Integrerat modellsystem för vattenkvalitetsberäkningar

88 Pia Andersson (2007)
Ballast Water Exchange areas – Prospect of designating BWE areas in the Skagerrak and the Norwegian Trench

89 Anna Edman, Jörgen Sahlberg, Niclas Hjerdt, Eleonor Marmefelt och Karen Lundholm (2007)
HOME Vatten i Bottenvikens vatten-distrikt. Integrerat modellsystem för vattenkvalitetsberäkningar

90 Niclas Hjerdt, Jörgen Sahlberg, Eleonor Marmefelt och Karen Lundholm (2007)
HOME Vatten i Bottenhavets vattendistrikt. Integrerat modellsystem för vattenkvalitets-beräkningar

91 Elin Almroth, Morten Skogen, Ian Sehsted Hansen, Tapani Stipa, Susa Niiranen (2008)
The year 2006
An Eutrophication Status Report of the North Sea, Skagerrak, Kattegat and the Baltic Sea
A demonstration Project

92 Pia Andersson, editor and co-authors Bertil Håkansson*, Johan Håkansson*, Elisabeth Sahlsten*, Jonathan Havenhand**, Mike Thorndyke**, Sam Dupont** * Swedish Meteorological and Hydrological Institute ** Sven Lovén, Centre of Marine Sciences (2008)
Marine Acidification – On effects and monitoring of marine acidification in the seas surrounding Sweden

93 Jörgen Sahlberg, Eleonor Marmefelt, Maja Brandt, Niclas Hjerdt och Karen Lundholm (2008)
HOME Vatten i norra Östersjöns vatten-distrikt. Integrerat modellsystem för vattenkvalitetsberäkningar.

94 David Lindstedt (2008)
Effekter av djupvattenomblandning i Östersjön – en modellstudie

95 Ingemar Cato*, Bertil Håkansson**, Ola Hallberg*, Bernt Kjellin*, Pia Andersson**, Cecilia Erlandsson*, Johan Nyberg*, Philip Axe** (2008)
*Geological Survey of Sweden (SGU)
**The Swedish Meteorological and Hydrological Institute (SMHI)

A new approach to state the areas of oxygen deficits in the Baltic Sea

96 Kari Eilola, H.E. Markus Meier, Elin Almroth, Anders Höglund (2008)
Transports and budgets of oxygen and phosphorus in the Baltic Sea

97 Anders Höglund, H.E. Markus Meier, Barry Broman och Ekaterini Kriezi (2009)
Validation and correction of regionalised ERA-40 wind fields over the Baltic Sea using the Rossby Centre Atmosphere model RCA3.0

98 Jörgen Sahlberg (2009)
The Coastal Zone Model

99 Kari Eilola (2009)
On the dynamics of organic nutrients, nitrogen and phosphorus in the Baltic Sea

100 Kristin I. M. Andreasson (SMHI), Johan Wikner (UMSC), Berndt Abrahamsson (SMF), Chris Melrose (NOAA), Svante Nyberg (SMF) (2009)
Primary production measurements – an intercalibration during a cruise in the Kattegat and the Baltic Sea

101 K. Eilola, B. G. Gustafson, R. Hordoir, A. Höglund, I. Kuznetsov, H.E.M. Meier T. Neumann, O. P. Savchuk (2010)
Quality assessment of state-of-the-art coupled physical-biogeochemical models in hind cast simulations 1970-2005

102 Pia Andersson (2010)
Drivers of Marine Acidification in the Seas Surrounding Sweden

103 Jörgen Sahlberg, Hanna Gustavsson (2010)
HOME Vatten i Mälaren

104 K.V Karmanov., B.V Chubarenko, D. Domnin, A. Hansson (2010)
Attitude to climate changes in everyday management practice at the level of Kaliningrad region municipalities

105 Helén C. Andersson., Patrik Wallman, Chantal Donnelly (2010)
Visualization of hydrological, physical and biogeochemical modelling of the Baltic Sea using a GeoDome™

106 Maria Bergelo (2011)
Havsvattenståndets påverkan längs Sveriges kust – enkätsvar från kommuner, räddningstjänst, länsstyrelser och hamnar

107 H.E. Markus Meier, Kari Eilola (2011)
Future projections of ecological patterns in the Baltic Sea

108 Meier, H.E.M., Andersson, H., Dieterich, C., Eilola, K., Gustafsson, B., Höglund, A., Hordoir, R., Schimanke, S (2011)
Transient scenario simulations for the Baltic Sea Region during the 21st century

109 Ulrike Löptien, H.E. Markus Meier (2011)
Simulated distribution of colored dissolved organic matter in the Baltic Sea

110 K. Eilola[1], J. Hansen[4], H. E. M. Meier[1], K. Myrberg[5], V. A. Ryabchenko[3] and M. D. Skogen[2] (2011)
[1]Swedish Meteorological and Hydrological Institute, Sweden, [2] Institute of Marine Research, Norway, [3] St. Petersburg Branch, P.P.Shirshov Institute of Oceanology, Russia, [4] National Environmental Research Institute, Aarhus University, Denmark, [5]Finnish Environment Institute, Finland
Eutrophication Status Report of the North Sea, Skagerrak, Kattegat and the Baltic Sea: A model study
Years 2001-2005

SMHI

Swedish Meteorological and Hydrological Institute
SE 601 76 NORRKÖPING
Phone +46 11-495 80 00 Telefax +46 11-495 80 01

ISSN 0283-7714